

1 **Response of seasonal soil freeze depth to climate change across China**

2 Xiaoqing Peng^{1,2}, Oliver W. Frauenfeld², Tingjun Zhang^{1*}, Kang Wang³, Bin Cao^{1,4}, Xinyue
3 Zhong⁵, Hang Su¹, Cuicui Mu¹

4 ¹ Key Laboratory of Western China's Environmental Systems (Ministry of Education), College of
5 Earth and Environmental Sciences, Lanzhou University, Lanzhou, 730000, China

6 ² Department of Geography, Texas A&M University, College Station, TX 77843-3147, USA

7 ³ Institute of Arctic and Alpine Research, University of Colorado at Boulder, Boulder, CO 80309,
8 USA

9 ⁴ Department of Geography & Environmental Studies, Carleton University, Ottawa, Ontario,
10 Canada

11 ⁵ Northwest Institute of Eco-Environment and Resources, Chinese Academy of Sciences, Lanzhou
12 730000, China

13 * *Correspondence to:* Tingjun Zhang (tjzhang@lzu.edu.cn)

14 **Abstract.** The response of seasonal soil freeze depth to climate change has repercussions for the
15 surface energy and water balance, ecosystems, the carbon cycle, and soil nutrient exchange.

16 Despite its importance, **the response of soil freeze depth to climate change is largely unknown.**

17 **This study employs the Stefan solution, and observations from 845 meteorological stations to**
18 investigate the response of variations in soil freeze depth to climate change across China.

19 Observations include daily air temperatures, daily soil temperatures at various depths, mean
20 monthly gridded air temperatures, and the Normalized Difference Vegetation Index. Results show

21 that soil freeze depth decreased significantly at a rate of -0.18 ± 0.03 cm/year, resulting in a net
22 decrease of 8.05 ± 1.5 cm over 1967–2012 across China. On the regional scale, soil freeze depth

23 decreases varied between 0.0 and 0.4 cm/year in most parts of China during 1950-2009.

24 **Investigating potential climatic and environmental driving factors of soil freeze depth**

25 **variability, we find that mean annual air temperature and ground surface temperature, air**
26 **thawing index, ground surface thawing index, and vegetation growth are all negatively**

27 **associated with soil freeze depth. Changes in snow depth are not correlated with soil freeze**

28 **depth. Air and ground surface freezing index are positively correlated with soil freeze depth.**

29 **Comparing these potential driving factors of soil freeze depth, we find that freezing index**

30 **and vegetation growth are more strongly correlated with soil freeze depth, while snow depth**
31 **is not significant.** We conclude that air temperature increases are responsible for the decrease in
32 seasonal freeze depth. These results are important for understanding the soil freeze/thaw dynamics
33 and the impacts of soil freeze depth on ecosystem and hydrological process.

34 **1 Introduction**

35 **Combining multiple land and ocean surface temperature datasets, the global mean**
36 **air temperature increased 0.85 °C over 1880-2012 (Stocker et al., 2014).** Given that all of the
37 cryosphere's components are inherently sensitive to air temperature changes on different time
38 scales, cryospheric changes serve as indicators of climate change. Frozen ground is an important
39 component of the cryosphere. Permafrost regions underlay approximately 24% of the exposed
40 land surface of the Northern Hemisphere (Zhang et al., 1999), and seasonally frozen ground (SFG)
41 regions occupy 57% (Zhang et al., 2003). China has the third-largest frozen ground extent in the
42 world, with a permafrost area of $\sim 2.20 \times 10^6$ km², or approximately 23% of its land area, mainly on
43 the Tibetan Plateau; regions with SFG occupy **about 50%** of the land area in China (Zhou et al.,
44 2000). Under warming climate conditions, frozen ground regions are vulnerable to subsidence,
45 especially ice-rich permafrost and relatively warm discontinuous permafrost (Morison et al., 2000;
46 Osterkamp et al., 2000; Stendel and Christensen, 2002). Maximum soil freeze depth of SFG and
47 active layer depth over permafrost play a significant role in cold environments, and all
48 hydrological, ecological, biological, and pedological activities occur within this layer (Hinzman et
49 al., 1991; Kane et al., 1991; Zhao et al., 2004). Simultaneously, soil freeze depth influences the
50 surface and subsurface hydrologic cycle, promotes soil texture changes, and alters the availability
51 of soil nutrients for plant growth. The soil freeze/thaw cycle and soil freeze depth variations affect
52 the decomposition of soil organic matter and greenhouse gas exchanges between the land surface
53 and the atmosphere (Shiklomanov and Nelson, 2002; Mu et al., 2015; **Jafarov and Schaefer,**
54 **2016).** Thus, seasonal soil freeze depth variability and climate are closely linked.

55 Due to global climate warming, significant efforts have been devoted to permafrost
56 research, such as permafrost variations on the hemispheric-scale, permafrost temperature changes
57 (Wu and Zhang, 2008; Romanovsky et al., 2010; Guglielmin and Cannone, 2012; Streletskiy et al.,
58 2014; Wu et al., 2015), permafrost degradation (Jorgenson et al., 2006; Ravanel et al., 2010;

59 Sannel and Kuhry, 2011; Streletskiy et al., 2015; Park et al., 2016), hydrological processes in
60 permafrost regions (Hu et al., 2009; Wang et al., 2009; Park et al., 2013; Streletskiy et al., 2015;
61 Ford and Frauenfeld, 2016), feedbacks to climate change (Schuur et al., 2008; Park et al., 2015;
62 **Abbott et al., 2016**), and other aspects. The increasing thickness of the active layer has been
63 indicated by many observations in permafrost regions at high latitudes (Brown et al., 2000;
64 Frauenfeld et al., 2004; Zhang et al., 2005; Fyodorov-Davydov et al., 2008; Smith et al., 2010; Wu
65 and Zhang, 2010; Zhao et al., 2010; Callaghan et al., 2011; Li et al., 2012; Liu et al., 2014;
66 Stocker et al., 2014). Less research has focused on SFG areas (Zhang et al., 2003; Frauenfeld et al.,
67 2004; Frauenfeld and Zhang, 2011; Wang et al., 2015), although the near-surface soil freeze/thaw
68 status has been investigated using satellite passive microwave remote sensing (Zhang and
69 Armstrong, 2001; Zhang et al., 2003, 2004; Li et al., 2008; Jin et al., 2015). **Peng et al. (2016)**
70 **analyzed the response of soil freeze/thaw states to climate change across China, based on**
71 **observational data. While Peng et al. (2016) investigated the area extent changes of different**
72 **soil freeze/thaw states, here we instead focus on seasonal soil freeze depth. Regional-scale soil**
73 **freeze depth can be an important indicator of climate change and frozen ground condition in**
74 **cold regions. Further, SFG is closely related with human activities, because most populated**
75 **areas are located on SFG.**

76 Shiklomanov (2012) similarly pointed out that SFG has not received much attention
77 despite its vast area extent and importance, mainly due to a lack of long-term observational time
78 series to document changes. Evaluating climatic and **environmental** changes on SFG requires
79 comprehensive spatial assessments of available soil temperature records (Shiklomanov, 2012). To
80 date, no comprehensive investigation of soil freeze depth in relation to climate change has been
81 conducted in China, despite the prevalence of SFG in this part of the world. Therefore, using
82 long-term observational data, the goals and unique contributions of this study are 1) to estimate
83 the spatial and temporal variations of seasonal soil freeze depth across China; 2) to quantify the
84 potential forcing factors of soil freeze depth including climatic and **environmental** factors; and 3)
85 to establish how soil freeze depth variability responds to climate change in China.

86 **2 Data and methods**

87 **2.1 Data**

88 **Several datasets are used including daily air and ground surface temperature, daily**
89 **soil temperature at 0-320 cm depth, mean monthly gridded air temperature, and daily snow**
90 **depth. In addition, we incorporate a 1-km resolution digital elevation model (DEM) and**
91 **normalized differential vegetation index (NDVI) data. All datasets are described in detail**
92 **below.**

93 **2.1.1 Mean daily air and ground surface temperature**

94 Mean daily air temperature and ground surface temperature data are collected from the
95 China Meteorological Administration (CMA) for a total of 839 meteorological stations (Figure 1)
96 available four times daily at 02:00, 08:00, 14:00, and 20:00 (<http://cdc.cma.gov.cn/>; Wang et al.,
97 **2015**). These data come already quality controlled, and station observations date back to the 1950s
98 and 1960s. Some stations end during the 1990s, while others are available until 2013. Most
99 stations are located in east central China, with fewer sites in the west and at high elevations, such
100 as on the Qinghai-Tibetan Plateau (Figure 1). These mean daily air and ground surface
101 temperatures are used to estimate temperature changes and to calculate the freeze/thaw index.

102 **2.1.2 Soil temperature**

103 Daily soil temperature data are available for 845 sites across China (Figure 1) from the
104 CMA, measured at the depths of 0.00, 0.05, 0.1, 0.15, 0.2, 0.4, 0.5, 0.8, 1.6, and 3.2 m. The
105 temporal record varies for these stations, with some observations dating back to the late 1950s,
106 and some only to the 1970s. Some station records end in the 1990s, while others are available
107 through 2006 (Wang et al., 2015). Soil temperature is used to calculate the soil freeze depth; **we**
108 **combine the potential maximum soil seasonal freeze depth in permafrost regions, and the**
109 **maximum soil freeze depth in SFG.** The number of stations with both daily air temperature and
110 soil temperature observations is 729.

111 **2.1.3 Mean monthly gridded air temperature**

112 Mean monthly gridded air temperature (MMGAT) was used to analyze soil freeze depth
113 at the regional scale across China. We obtained the University of Delaware's 1900–2014 terrestrial
114 air temperature gridded monthly time series (<http://climate.geog.udel.edu/~climate/>), with a
115 $0.5^\circ \times 0.5^\circ$ spatial resolution. This dataset was produced by combining many observational station
116 records across the world, using spatial interpolation and cross-validation procedures (Legates et al.,

117 1990; Willmott et al., 1995; Peterson et al., 1997, 1998). **MMGAT during 1950–2010 is used for**
118 **assessing its correspondence with seasonal freeze depth across China.**

119 **2.1.4 Digital elevation model (DEM)**

120 **Considering the complex terrain across China and the impacts of elevation on air**
121 **temperature, we also used the global 30 arc-second elevation dataset (GTOPO30;**
122 **<https://lta.cr.usgs.gov/GTOPO30>) as the digital elevation model (DEM) for this study to**
123 **further improve the MMGAT resolution. GTOPO30 was derived from several raster and**
124 **vector sources of topographic information. Across China, the elevation ranges from –152 to**
125 **8752 m (Figure 1). Based on this DEM, we spatially interpolate the MMGAT data to the**
126 **DEM’s 30 arc-second (1-km) resolution.**

127 **2.1.5 Snow depth**

128 **We obtained daily mean snow depth data for 672 sites across China (Che et al., 2008).**
129 **The period of record at these locations varies, with some stations dating back to the late 1950s and**
130 **some only to the 1970s. Some station records end around the 1990s while others are available**
131 **through 2005. The snow depth was used to assess its influence on soil freeze depth. We calculate**
132 **the annual maximum snow depth (SND) from the daily data for 1 July–30 June, and match**
133 **those snow depth stations with the soil temperature stations. If there are missing data in the**
134 **spring, autumn, and winter season of one station, this station data will not be used.**

135 **2.1.6 Normalized differential vegetation index (NDVI)**

136 **The NDVI dataset used in this study is produced by the Global Inventory Modeling and**
137 **Mapping Studies (GIMMS) team, available for 1982–2006. It is derived from NOAA AVHRR**
138 **data, available at 15-day temporal resolution and an 8-km spatial resolution (Tourre et al., 2008).**
139 **These data were used to assess the influence of vegetation on soil freeze depth. We extracted**
140 **the NDVI values corresponding to the stations’ latitude and longitude coordinates.**

141 **2.2 Methods**

142 **Missing data often present a potential problem for analyzing and averaging time**
143 **series. Therefore, if fewer than five days were missing in a given month, filling in missing**
144 **daily air temperatures was based on highly correlated neighboring sites using linear**
145 **regression. Missing daily mean ground surface temperatures were estimated through linear**

146 **regression with the daily mean air temperature at the same station. Based on the daily air**
147 **temperature, we also calculate the mean monthly air temperature and mean annual air**
148 **temperature (MAAT). The interpolated results are strongly correlated with observations, as**
149 **indicated by regression coefficients larger than 0.95.**

150 To improve the original $0.5^\circ \times 0.5^\circ$ MMGAT data to a 1-km resolution, spatial
151 interpolation was used in conjunction with monthly lapse rates and the 1-km resolution DEM (e.g.,
152 Willmott and Matsuura, 1995; Gruber et al., 2012). The data processing steps are to (1) calculate
153 the average monthly atmospheric lapse rate based on all available meteorological stations across
154 China and their elevations; (2) bring each average monthly gridded air temperature value to a
155 **reference level (elevation of 0 m)** using the average monthly lapse rate; (3) apply a Kriging
156 interpolation to the reference-level adjusted MMGAT; and (4) bring the gridded reference-level air
157 temperature back to the DEM-gridded height. Based on more than 800 sites, we evaluated the
158 interpolated MMGAT against the observational monthly air temperatures, and find that the
159 regression coefficient is almost 1.0 with a minimum of 0.98 in April.

160 The freezing/thawing index can also be an important indicator to assess the variations in
161 frozen ground (Zhang et al., 1997; Nelson, 2003; Frauenfeld et al., 2007). There are two primary
162 types of freezing/thawing indices: the surface freezing/thawing index, calculated from ground
163 surface temperatures, and the air freezing/thawing index, computed from air temperatures. **To**
164 **calculate the freezing index, we sum all temperatures below 0 °C during the freezing periods**
165 **(equation 1), and similarly calculate the thawing index by summing the above-0 °C**
166 **temperatures during the warm season (equation 2; Wu et al., 2011; Luo et al., 2014). We**
167 **define the freezing period to be July–June, to sum the freezing index over a continuous cold**
168 **season (equation 1). The warming period is defined as the calendar year (Wu et al., 2011;**
169 **Peng et al., 2013, 2016) (equation 1, 2). Thus, freezing/thawing index at the point scale was**
170 **calculated based on the daily mean air temperatures and ground surface temperatures. For the**
171 regional-scale air freezing index, we use the adjusted 1-km gridded terrestrial air temperature data.

$$FI = \sum_{i=1}^{N_F} |T_i|, T_i < 0^\circ\text{C} \quad (1)$$

$$TI = \sum_{i=1}^{N_T} T_i, T_i > 0^\circ\text{C} \quad (2)$$

172 where N_F is the number of days with temperature below 0°C ; $i = 1, 2 \dots N_F$; N_T is the number of
 173 days with temperatures above 0°C ; and T_i represents the temperature on a specific day.

174 Various methods are available to calculate the soil freeze depth. For example, it can be
 175 estimated directly from soil temperature, from physical and statistical models, and based on the
 176 Stefan solution. In this study, we use the Stefan solution to estimate soil freeze depth, which is
 177 determined using equation 3:

$$SFD = \sqrt{2K_f \left(\frac{n_f FI_a}{P_b w L} \right)} \quad (3)$$

178 where SFD is soil freeze depth (m), K_f is the thermal conductivity of the frozen soil ($\text{W/m} \cdot ^\circ\text{C}$), n_f
 179 is the n-factor for the freezing season and corresponds to the ratio between the surface freezing
 180 index and the air freezing index (Peng et al., 2016), FI_a is the annual air freezing index ($^\circ\text{C} \cdot \text{d}$), P_b
 181 is the soil bulk density (kg/m^3), w the soil water content by weight, and L the latent heat of fusion
 182 (J/kg) (Zhang et al., 2005). In equation 3, many site-specific factors are required to estimate SFD,
 183 which are generally not available, particularly at the regional scale. **However, based on the SFD**
 184 **and annual freezing index at each observational site, we can quantify the relationship**
 185 **between these two parameters (Figure 2). We find a strong and statistically significant**
 186 **correlation of $R=0.87$.** Thus, the relationship between SFD and the annual freezing index can be
 187 simplified (Harlan and Nixon, 1978) as:

$$SFD = E \sqrt{FI_a} \quad (4)$$

188 where E is defined (Nelson and Outcalt, 1987) as:

$$E = \sqrt{\frac{2K_f n_f}{P_b w L}} \quad (5)$$

189 To estimate the SFD at the regional scale across China, we first calculate SFD for every
 190 observational station by interpolating the depth of the 0°C isotherm throughout the 0.0–3.2 m soil
 191 profile using the daily mean soil temperature (Frauenfeld et al., 2004). Next, we estimate the FI_a
 192 based on the calculations in Frauenfeld et al. (2007). To estimate the E value for all stations, we

193 use the SFD, FI_a , and equations 2 and 3. Then, we interpolate the E value to the regional scale at
194 1-km resolution using kriging in ArcGIS. The SFD is estimated across China based on equation 4,
195 the 1-km E value, and FI_a . We can then estimate the regional-scale SFD for each year from 1950
196 to 2009 across China, and obtain the mean decadal SFD. Finally, we estimate the SFD trend at the
197 regional scale across China based on regression analysis.

198 From the 1-km scale E factor values, we can extract every site's E factor based on the
199 sites' latitude and longitude. Then, the air freezing index from the sites is used to calculate the
200 annual soil freeze depth at every site by equation 4. To evaluate the result, we compare the
201 observational SFD calculated from the soil temperatures, and the simulated SFD derived from the
202 Stefan method (equation 4) in figure 3. The result demonstrates that the mean absolute error and
203 root-mean-square error are 0.08 m and 0.14 m, respectively, indicating that there is a good
204 agreement between simulated and observational SFD.

205 **A number of climatic and environmental variables including MAAT, mean annual**
206 **ground surface temperature (MAGST), freezing index, thawing index, SND, and NDVI are**
207 **selected to investigate the potential drivers of the observed long-term SFD changes across**
208 **China.** We use Pearson correlations to analyze the association between these variables and SFD,
209 and employ a 95%-significance level to assess the statistical significance for all analyses.

210 **3 Results**

211 **3.1 Soil freeze depth**

212 Figure 4 shows the spatial variability and trends of SFD at every location. The highest
213 SFD was mainly located in northeastern and northwestern China, and the Tibetan Plateau. In
214 contrast, the lowest SFD was found in the south of China. Locations with SFD greater than 0.4 m
215 are found north of the Yellow River. In the northwest of China, locations with SFD less than 0.8 m
216 are found in the Taklimakan desert, and some sites with SFD greater than 2.0 m are located in the
217 Altai, Tianshan, and Pamir Mountains.

218 On the Tibetan Plateau, most sites have a SFD greater than 2.4 m. There is an increase in
219 SFD with increasing latitude and elevation. The significant SFD changes are between -0.4 and less
220 than 0 cm/year. The sites with the strongest decreasing trends of -1.2 cm/year are on Tibetan
221 Plateau and -1.0 cm/year in the north of China.

222 **Figure 5 shows the standard deviation of SFD at each site across China. It varies**
223 **from 0.00–0.27 m. The standard deviation of SFD is generally less than 0.03 m south of 35°N,**
224 **except on the Tibetan Plateau. In northeastern China, the standard deviation changes**
225 **between 0.06 m and 0.15 m. In the northwest, it is generally 0.06–0.12 m. On the Tibetan**
226 **Plateau, the standard deviation varies from less than 0.09 m, but can be greater than 0.18 m**
227 **at some sites.**

228 Based on the sites' E factors and FI_a , we calculate SFD time series anomalies from 1951
229 to 2012 (Figure 6). Although a composite time series of all available stations data can be
230 calculated during 1951–2012, few of 839 stations actually contribute to the mean values before the
231 1960s (Figure 6). There are fewer than 200 stations in the early years, which therefore does not
232 represent the SFD across China as a whole. Beginning in 1967, more than 800 stations contribute
233 to each year's mean, therefore long-term SFD trends will only be evaluated from then on. There is
234 a statistically significant change in SFD anomalies of -0.18 ± 0.03 cm/year, corresponding to a net
235 decrease of 8.05 ± 1.5 cm. In addition to the overall long-term decrease, there are also some
236 patterns of inter-decadal variability during 1967–2012, including slight positive changes in some
237 periods. SFD exhibited both increases and decreases until 1975, followed by a sharp decrease until
238 1990. However, SFD has remained constant or may perhaps be increasing slightly during
239 1990–2012. Therefore, the overall SFD change during 1967–2012 was largely controlled by the
240 decrease during 1975–1990. Similar SFD changes, attributable to variability in the North Atlantic
241 Oscillation, were found in high-latitude Eurasia (Frauenfeld and Zhang, 2011).

242 **3.2 Spatial and temporal variability of SFD in China**

243 Based on the 1-km resolution E factor and 1-km FI_a calculated from MMGAT, we
244 estimate SFD across China from 1950 to 2009 by the Stefan method. Figure 7 shows the spatial
245 variability of mean decadal SFD. The overall spatial pattern of SFD variability is quite consistent.
246 Thus, we describe the spatial pattern of SFD from the 1950s as an example. SFD increases with
247 latitude and elevation, with SFD greater than 1.5 m in northeastern China, the Mongolia Plateau,
248 Tibetan Plateau, and north of the Xinjiang region. In the east of China, the SFD ranges from 0.0 m
249 to more than 4.0 m, and increases with latitude. In the Yellow River region, the elevation
250 decreases from west to east, while the SFD varies from greater than 2.5 m to less than 0.5 m. The

251 SFD in the Taklimakan desert is lower than in the surrounding area.

252 Figure 8 represents the SFD trend across China from 1950 to 2009. The gray region
253 represents areas where the SFD trends are not statistically significant, however, they are
254 statistically significant in all other regions. In general, the SFD decreased significantly over
255 northern China, except in two small areas. The SFD trend ranges between 0.0 and -0.4 cm/year in
256 most areas. SFD trends less than -0.4 cm/year are found in some areas, such as the Tibetan Plateau,
257 and the Pamirs. In the two small areas of increasing SFD, we further investigated the MAAT trend
258 during 1950-2010 based on the MMGAT dataset. There is similarly a statistically significant
259 decrease of MAAT in these same areas during this period. Therefore, air temperature is possibly
260 one of the important factors that influence SFD in these areas. **More detailed discussion is**
261 **provided in sections 3.3 and 4.1.**

262 Overall, the spatial variability indicates that SFD changes with latitude and elevation at
263 the regional scale across China. As is expected from climate warming, a statistically significant
264 decreasing trend in SFD is evident across China from 1950 to 2009.

265 **3.3 Potential forcing variables**

266 To explore the possible variables leading to the documented changes in SFD, we analyze
267 potentially important factors for soil freeze dynamics: MAAT, MAGST, freezing index including
268 FI_a and the ground surface freezing index (FI_s), thawing index including the air (TI_a) and ground
269 surface thawing index (TI_s), SND, and NDVI. Temperature—including MAGST and MAAT—at
270 the 839 station locations exhibits a statistically significant increase over the 1951–2013 period of
271 0.019 and 0.013 °C/year, or approximately 1.2 °C and 0.78 °C over the 63 years, respectively
272 (Figure 9 a, and b). MAGST and MAAT are statistically significantly correlated with SFD at
273 $R=-0.56$ and $R=-0.66$, which means that 31% and 44%, respectively, of the variability in SFD can
274 be accounted for by these temperature measures. Further, the negative correlation demonstrates
275 that increasing temperatures result in SFD decreases at the 839 stations.

276 Soil freeze usually begins in autumn or winter, with temperatures less than 0 °C reaching
277 their maximum freeze depth toward the end of winter season or spring. Therefore, maximum
278 annual SFD occurs during the cold seasons. Freezing index is an important indicator for
279 accumulated cold season temperatures (Frauenfeld and Zhang, 2011). From 1951 to 2013, FI_s and

280 FI_a underwent a statistically significant decrease of 3.0 and 1.62 °C-days/year, respectively
281 (Figure 9 c, and d), indicating warming, which reduces the cold season's magnitude and/or
282 duration. The correlation between FI_s , FI_a , and SFD was a statistically significant 0.68 and 0.87,
283 indicating that the FI accounts for 46% and 76% of SFD variability.

284 The thawing index is used to assess the accumulated positive degree-days during the
285 warm season (Frauenfeld and Zhang, 2011). There are no obvious TI changes at the station
286 locations until approximately 1985. TI increases during 1985-2008, followed by a decrease until
287 2013. From 1951 to 2013, TI_s and TI_a show statistically significant increases at a magnitude of
288 3.73 and 2.77 °C-days/year, respectively (Figure 9 e and f). The correlation coefficient between
289 TI_s , TI_a , and SFD is -0.53 and -0.57, respectively, indicating a weak negative association, such that
290 warm summer conditions correspond to a shallower SFD the following cold season.

291 Figure 10 shows the correlation between SFD and SND. **However, the weak negative**
292 **correlation between SFD and SND of $R=-0.13$ is not statistically significant, indicating that**
293 **there is no relationship. This result is also consistent with the findings of Jafarov and**
294 **Schaefer (2016).**

295 As suggested by Shiklomanov (2012), **environmental** factors likely also affect SFD. The
296 surface can be affected directly by climate forcing, while the subsurface effects are more complex.
297 The subsurface soil only indirectly receives a climatic signal, which is furthermore altered by
298 site-specific soil processes (e.g., thermal conductivity and analogous soil properties). Vegetation is
299 a likely **environmental** factor that influences the soil freeze depth (Shiklomanov, 2012). Thus, we
300 investigate vegetation using NDVI (Peng et al., 2013) and find it is significantly correlated with
301 SFD at -0.80, suggesting that 64% of the variability in SFD can be accounted for by NDVI. The
302 statistically significant negative correlation demonstrates that when NDVI increases (greening),
303 this corresponds to a decrease in SFD (Figure 11).

304 **4 Discussion**

305 Soil freeze/thaw depth changes involve a series of interactions, such as energy exchanges,
306 soil moisture exchanges, and gas exchanges between the atmospheric and terrestrial system.
307 Therefore, variations of soil freeze/thaw most likely have an important effect on geomorphic,
308 hydrological, and biological processes. **Similarly, soil freeze/thaw depth changes also have**

309 **destabilizing effects on engineering structures, such as on improperly constructed**
310 **infrastructure** (Smith and Burgess, 1999; Stendel and Christensen, 2002). The release of
311 additional greenhouse gases to the atmosphere also occurs (Michaelson et al., 1996; Mu et al.,
312 2015). In this paper, we use the Stefan method to calculate SFD, analyze the spatial SFD
313 variability and trends, and quantify the potential driving factors affecting SFD.

314 **4.1 Climatic and environmental factors**

315 **SFD variability is susceptible to climate warming and environmental change, and is**
316 **affected by variables including air temperature, ground surface temperature,**
317 **freezing/thawing index, and vegetation.** Many examples of permafrost degradation have been
318 reported, such as deeper the active layer thickness, reduced freeze time duration, and shifts in the
319 timing of thawing and freezing in seasonally frozen ground regions (Henry, 2008; Callaghan et al.,
320 2011; Stocker et al., 2014; Wang et al., 2015). Negative correlations are found here between SFD
321 and temperature (including MAAT and MAGST), because of solar radiation heating the ground,
322 energy transfer into the soil, ultimately increasing the soil temperature. Thus, increasing
323 temperature is found to be the main factor influencing SFD variability in China, as in previous
324 work focusing only on the Tibetan Plateau (Zhao et al., 2004).

325 The freezing/thawing indices represent the accumulated negative and positive
326 degree-days in the cold and warm seasons, respectively (Wu et al., 2011). The positive and
327 negative correlation between SFD and FI and TI were statistically significant, consistent with
328 previous results in other regions (Frauenfeld and Zhang, 2011). Due to the maximum soil freeze
329 depth occurring in the cold season and SFD being affected by temperature, the positive correlation
330 between SFD and FI is reasonable. Although TI is the accumulated temperature in the warm
331 season, it takes some time to transfer the energy into the deeper ground. The energy flux into the
332 soil reduces with increasing soil depth. Therefore, if all the conditions are the same, a larger TI can
333 precondition the ground by increasing the energy in the deeper soil, which can subsequently delay
334 soil freezing. **Thus TI is a potential indicator of SFD, indirectly affecting soil temperature**
335 (Frauenfeld and Zhang, 2011).

336 Snow depth can have an effect on soil temperature, which would affect the active layer
337 thickness and seasonal SFD variability. Numerical modeling studies have shown that snow depth

338 does impact SFD (Zhang and Stamnes, 1998; Ling and Zhang, 2003; Park et al., 2015). Park et al.
339 (2015) indicated that both increasing SND and snow structure (e.g., snow density) changes were
340 favorable to soil warming, resulting in active layer thickness decreasing in northern regions as
341 previously found by Frauenfeld et al. (2004). Snow cover insulates the ground during the cold
342 season (Zhang, 2005). Interestingly, in our study we did not find a relationship between SND and
343 SFD. This could be due to the spatial heterogeneity of snow across China. According previous
344 research, snow depth, snow water equivalent, and snow densities are smallest on the Tibetan
345 Plateau compared to other parts of China (Ma et al., 2012). Compared with other regions,
346 multi-year average snow depth in general is low in China, especially on the Tibetan Plateau and
347 the east-central mountain regions of China (Zhong et al., 2014), and may therefore have only
348 limited insulating effects. This could lead to the lack of a relationship between SFD and SND
349 across China and motivates further future investigation.

350 **A negative correlation between SFD and vegetation, as quantified by NDVI, is found.**
351 **Vegetation change has a significant influence on the climate system mostly through changes**
352 **to the surface radiative energy budget, which can be affected the SFD. Based on previous**
353 **research, vegetation varies in different land cover types and responds to climate change via**
354 **different physical mechanisms (Snyder et al., 2004), e.g., changes in the surface albedo (e.g.,**
355 **bare ground versus vegetation cover), vegetation transpiration, and shading effects (Kelley**
356 **et al., 2004; Snyder et al., 2004; Swann et al., 2010; Chang et al., 2012; Zhang et al., 2012). In**
357 **the cold season, less/decreased vegetation will be more easily snow covered, thus increasing**
358 **the albedo considerably. Increasing albedo results in less net radiation at the land surface, as**
359 **more incoming solar radiation is reflected from the surface. Then, the surface air**
360 **temperature will decrease considerably due to less energy absorbed at the surface. For the**
361 **colder land surface, the sensible heat flux is reduced. Further, the vegetation decrease results**
362 **in reducing evapotranspiration, which decreases the latent heat flux (Snyder et al., 2004).**
363 **Compared to increased vegetation cover, less vegetation causes a large annual-average**
364 **increase in the surface albedo with the largest changes in the winter and spring seasons,**
365 **which reduces the amount of net radiation at the surface, making the surface colder and**
366 **resulting in SFD increases. Conversely, vegetation increases could lead to decreasing SFD.**

367 The vegetation's effect on transpiration is primarily important in summer, while SFD
368 primary occurs in winter and spring (Snyder et al., 2004).

369 The significant negative correlation between NDVI and SFD demonstrates their
370 inverse relationship. Results from many previous studies indicated that there has been a
371 vegetation increase, or a greening trend, in different regions during the past several decades
372 (Peng et al., 2011; Piao et al., 2011; Zhang et al., 2013; Zhu et al., 2016). Because climate
373 change controls the spatial distribution of vegetation, most studies examine vegetation
374 variability as impacted by climate change, including temperature and precipitation (Bao et
375 al., 2015; Huang et al., 2016). Results showed that increasing temperature and precipitation
376 result in vegetation increases. Similarly, figure 8 shows that rising temperature results in a
377 SFD decrease. The negative relationship between SFD and NDVI indicates the effect of
378 vegetation on SFD, and also their inverse relationship.

379 SFD is affected by many factors, including the climatic and environmental variables
380 considered in this study. However, SFD changes in different regions are also potentially
381 influenced by many other local environmental variables or large-scale teleconnections. Thus,
382 it remains difficult to fully account for the spatial variations of SFD at the regional scale.

383 4.2 Soil Freeze Depth in Different Climate Zones

384 Our results indicate significant changes of SFD across China. To address the spatial
385 pattern of SFD changes, we divide the study area into five different zones, including tropical
386 monsoon (TPM), subtropical monsoon (SM), temperate monsoon (TM), temperate
387 continental (TC), and Qinghai-Tibetan Alpine (QTA) climate zones, which are categorized
388 by temperature, precipitation, and other parameters. Results indicate that the 30-year
389 (1971-2000) average SFD in the SM, TM, TC, and QTA climate zones are 2.8 ± 0.5 cm,
390 113.6 ± 7.6 cm, 132.5 ± 7.8 cm, and 165.8 ± 6.7 cm, respectively. Similar changes of SFD are
391 found across the TM (-0.27 ± 0.005 cm/year), TC (-0.26 ± 0.005 cm/year), and QTA
392 (-0.22 ± 0.004 cm/year) zones during 1950-2009, while there are no significant changes in the
393 SM region. This is likely due to the higher temperatures in SM climate zone (Fig. 12).
394 Although this study investigates a number of environmental and climatic driving variables
395 of SFD, the degree to which other potential factors (e.g., soil texture, soil moisture, albedo,

396 **cloud cover, teleconnections) could also influence SFD remains unknown due to a lack of**
397 **reliable data.**

398 **5 Summary and Conclusions**

399 In this study, we conducted a comprehensive regional-scale investigation of SFD across
400 China. A significant climate indicator, SFD is influenced by many variables including climatic and
401 **environmental** factors. These factors are often integrated to affect SFD (Lachenbruch and
402 Marshall, 1986; Brown et al., 2000; Frauenfeld et al., 2004). Our results can be summarized as
403 follows:

404 The spatial distribution of SFD variability is influenced by latitude and elevation across
405 China. High latitude and altitude sites are characterized by large SFD. In contrast, smaller SFD
406 values are generally observed for lower latitude and lower elevation regions.

407 Of the total 839 sites, we find that the SFD decreased significantly, at -0.18 ± 0.03 cm/year
408 from 1967 to 2012, equal to a net change of 8.05 ± 1.5 cm. The long-term decrease also exhibits
409 inter-decadal variability, including some positive changes in some periods and no change since
410 1990.

411 On the regional scale, the 1950–2009 spatial variation of SFD ranges between 0.0 and
412 4.5 m across China, with most areas exhibiting significant decreases between less than 0.0 and
413 -0.4 cm/year. Different climatic and **environmental** factors were explored as potential driving
414 variables of SFD. A negative relationship is evident between SFD and MAAT, MAGST, TI_a , and
415 TI_s , with statistically significant correlations of -0.66 , -0.56 , -0.57 , and -0.56 , respectively. The
416 climatic factors FI_s and FI_a were correlated positively with SFD, at 0.87 and 0.68 , respectively.
417 There is no correlation between SFD and SND. The **environmental** factor vegetation (NDVI) is
418 negatively correlated with SFD, indicating that 64% of the changes in SFD can be accounted for
419 by vegetation. **Of the potential drivers of SFD explored here, FI and NDVI are most strongly**
420 **correlated with SFD in China, while no relationship is evident with SND.**

421

422 **Acknowledgments:** This study was funded by the National Natural Science Foundation of China
423 (grant No. 91325202, 41601063, 41671516), the National Key Scientific Research Program of
424 China (grant No. 2013CBA01802), and the Fundamental Research Funds for the Central

425 Universities (lzujbky-2015-217). We acknowledge computing resources and time at the
426 Supercomputing Center of Cold and Arid Region Environment and Engineering Research Institute
427 of Chinese Academy of Sciences.

428

429 **References**

- 430 **Abbott, B. W., Jones, J. B., Schuur, E. A., Chapin III, F. S., Bowden, W. B., Bret-Harte, M. S.**
431 **, Epstein, H. E., Flannigan, M. D., Harms, T. K., and Hollingsworth, T. N.: Biomass offsets**
432 **little or none of permafrost carbon release from soils, streams, and wildfire: an expert ass**
433 **essment, *Environmental Research Letters*, 11, 034014, doi: 10.1088/1748-9326/11/3/034014,**
434 **2016.**
- 435 **Bao, G., Bao, Y., Sanjjava, A., Qin, Z., Zhou, Y., and Xu, G.: NDVI-indicated long-term**
436 **vegetation dynamics in Mongolia and their response to climate change at biome scale,**
437 ***International Journal of Climatology*, 35, 4293-4306, doi: 10.1002/joc.4286, 2015.**
- 438 Brown, J., Hinkel, K., and Nelson, F.: The circumpolar active layer monitoring (calm) program:
439 Research designs and initial results, *Polar geography*, 24, 166-258, doi:
440 10.1080/10889370009377698, 2000.
- 441 Callaghan, T. V., Tweedie, C. E., and Webber, P. J.: Multi-decadal changes in tundra environments
442 and ecosystems: the International Polar Year-Back to the Future Project (IPY-BTF), *Ambio*, 40,
443 555-557, 2011.
- 444 **Chang, X. L., Jin, H. J., Wang, Y. P., Zhang, Y. L., Zhou, G. Y., Che, F. Q., and Zhao, Y. M.:**
445 **Influences of vegetation on permafrost: A review, *Acta Ecologica Sinica*, 32, 7981-7990, doi:**
446 **10.5846/stxb201202120181, 2012.**
- 447 **Che, T., Xin, L., Jin, R., Armstrong, R., and Zhang, T.: Snow depth derived from passive**
448 **microwave remote-sensing data in China, *Annals of Glaciology*, 49, 145-154, doi:**
449 **10.3189/172756408787814690, 2008.**
- 450 Christiansen, H. H., Etzelmüller, B., Isaksen, K., Juliussen, H., Farbrot, H., Humlum, O.,
451 Johansson, M., Ingeman-Nielsen, T., Kristensen, L., and Hjort, J.: The thermal state of
452 permafrost in the Nordic area during the International Polar Year 2007–2009, *Permafrost and*
453 *Periglacial Processes*, 21, 156-181, doi: 10.1002/ppp.687, 2010.
- 454 Ford, T. W. and Frauenfeld, O. W.: Surface–Atmosphere Moisture Interactions in the Frozen
455 Ground Regions of Eurasia, *Scientific reports*, 6, 19163, doi:10.1038/srep19163, 2016.
- 456 Frauenfeld, O. W. and Zhang, T.: An observational 71-year history of seasonally frozen ground
457 changes in the Eurasian high latitudes, *Environmental Research Letters*, 6, 044024, doi:
458 10.1088/1748-9326/6/4/044024, 2011.
- 459 Frauenfeld, O. W., Zhang, T., Barry, R. G., and Gilichinsky, D.: Interdecadal changes in seasonal
460 freeze and thaw depths in Russia, *Journal of Geophysical Research: Atmospheres*, 109, D05101,
461 doi: 10.1029/2003JD004245, 2004.
- 462 Frauenfeld, O. W., Zhang, T., and McCreight, J. L.: Northern Hemisphere freezing/thawing index
463 variations over the twentieth century, *International Journal of Climatology*, 27, 47-63, doi:
464 10.1002/joc.1372, 2007.
- 465 Fyodorov-Davydov, D., Kholodov, A., Ostroumov, V., Kraev, G., Sorokovikov, V., Davudov, S.,
466 and Merekalova, A.: Seasonal thaw of soils in the North Yakutian ecosystems, 481-486, doi:
467 10.13140/2.1.1928.1286, 2008.
- 468 Gruber, S.: Derivation and analysis of a high-resolution estimate of global permafrost zonation,
469 *Cryosphere*, 6, 221-233, doi: 10.5194/tc-6-221-2012, 2012.
- 470 Guglielmin, M. and Cannone, N.: A permafrost warming in a cooling Antarctica?, *Climatic*
471 *Change*, 111, 177-195, doi: 10.1007/s10584-011-0137-2, 2012.
- 472 Harlan, R. and Nixon, J.: Ground thermal regime, *Geotechnical engineering for cold regions*,
473 103-163, 1978.
- 474 Henry, H. A.: Climate change and soil freezing dynamics: historical trends and projected changes,
475 *Climatic Change*, 87, 421-434, doi: 10.1007/s10584-007-9322-8, 2008.
- 476 Hinzman, L., Kane, D., Gieck, R., and Everett, K.: Hydrologic and thermal properties of the active

477 layer in the Alaskan Arctic, *Cold Regions Science and Technology*, 19, 95-110, doi:
478 10.1016/0165-232x(91)90001-w, 1991.

479 Hu, H., Wang, G., Wang, Y., Liu, G., Li, T., and Ren, D.: Response of soil heat-water processes to
480 vegetation cover on the typical permafrost and seasonally frozen soil in the headwaters of the
481 Yangtze and Yellow Rivers, *Chinese Science Bulletin*, 54, 1225-1233, doi:
482 10.1007/s11434-008-0532-x, 2009.

483 **Huang, F., Mo, X., Lin, Z., and Shi, H.: Dynamics and responses of vegetation to climatic**
484 **variations in Ziya-Daqing basins, China, *Chinese Geographical Science*, 26, 478-494, doi:**
485 **10.1007/s11769-016-0807-0, 2016.**

486 **Jafarov, E. and Schaefer, K.: The importance of a surface organic layer in simulating permafrost**
487 **thermal and carbon dynamics, *The Cryosphere*, 10, 465-475, doi:**
488 **10.5194/tcd-9-3137-2015, 2016.**

489 Jin, R., Zhang, T., Li, X., Yang, X., and Ran, Y.: Mapping surface soil freeze-thaw cycles in China
490 based on SMMR and SSM/I brightness temperatures from 1978 to 2008, *Arctic, Antarctic, and*
491 *Alpine Research*, 47, 213-229, doi: 10.1657/AAAR00C-13-304, 2015.

492 Jorgenson, M. T., Shur, Y. L., and Pullman, E. R.: Abrupt increase in permafrost degradation in
493 Arctic Alaska, *Geophysical Research Letters*, 33, doi: 10.1029/2005GL024960, 2006.

494 Kane, D. L., Hinzman, L. D., and Zarling, J. P.: Thermal response of the active layer to climatic
495 warming in a permafrost environment, *Cold Regions Science and Technology*, 19, 111-122, doi:
496 10.1016/0165-232x(91)90002-x, 1991.

497 Kelley, A. M., Epstein, H. E., and Walker, D. A.: Role of vegetation and climate in permafrost
498 active layer depth in arctic tundra of northern Alaska and Canada, *Journal of Glaciology and*
499 *Geocryology*, 26, 269-274, 2004.

500 Lachenbruch, A. H. and Marshall, B. V.: Changing climate: geothermal evidence from permafrost
501 in the Alaskan Arctic, *Science*, 234, 689-696, doi: 10.1126/science.234.4777.689, 1986.

502 Legates, D. R. and Willmott, C. J.: Mean seasonal and spatial variability in gauge-corrected,
503 global precipitation, *International Journal of Climatology*, 10, 111-127, doi:
504 10.1002/joc.3370100202, 1990.

505 Li, R., Zhao, L., Ding, Y., Wu, T., Xiao, Y., Du, E., Liu, G., and Qiao, Y.: Temporal and spatial
506 variations of the active layer along the Qinghai-Tibet Highway in a permafrost region, *Chinese*
507 *Science Bulletin*, 57, 4609-4616, doi: 10.1007/s11434-012-5323-8, 2012a.

508 Li, X., Cheng, G., Jin, H., Kang, E., Che, T., Jin, R., Wu, L., Nan, Z., Wang, J., and Shen, Y.:
509 Cryospheric change in China, *Global and Planetary Change*, 62, 210-218, doi:
510 10.1016/j.gloplacha.2008.02.001, 2008.

511 Li, X., Jin, R., Pan, X., Zhang, T., and Guo, J.: Changes in the near-surface soil freeze-thaw cycle
512 on the Qinghai-Tibetan Plateau, *International Journal of Applied Earth Observation and*
513 *Geoinformation*, 17, 33-42, doi: 10.1016/j.jag.2011.12.002, 2012b.

514 Ling, F. and Zhang, T.: Numerical simulation of permafrost thermal regime and talik development
515 under shallow thaw lakes on the Alaskan Arctic Coastal Plain, *Journal of Geophysical Research:*
516 *Atmospheres*, 108, doi: 10.1029/2002jd003014, 2003.

517 Liu, L., Jafarov, E. E., Schaefer, K. M., Jones, B. M., Zebker, H. A., Williams, C. A., Rogan, J.,
518 and Zhang, T.: InSAR detects increase in surface subsidence caused by an Arctic tundra fire,
519 *Geophysical Research Letters*, 41, 3906-3913, doi: 10.1002/2014GL060533, 2014a.

520 Liu, L., Schaefer, K., Gusmeroli, A., Grosse, G., Jones, B. M., Zhang, T., Parsekian, A. D., and
521 Zebker, H. A.: Seasonal thaw settlement at drained thermokarst lake basins, Arctic Alaska,
522 *Atmospheric Chemistry and Physics*, 8, 815, doi: 10.5194/tc-8-815-2014, 2014b.

523 **Loveland, T. R., Reed, B. C., Brown, J. F., Ohlen, D. O., Zhu, Z., Yang, L., Merchant, J. W.:**
524 **Development of a global land cover characteristics database and IGBP discover from 1 km**
525 **AVHRR data. *International Journal of Remote Sensing*, 21, 1303-1330, doi:**
526 **10.1080/014311600210191, 2000.**

527 **Luo, D., Jin, H., Jin, R., Yang, X., and Lü, L.: Spatiotemporal variations of climate warming**
528 **in northern Northeast China as indicated by freezing and thawing indices, *Quaternary***
529 ***International*, 349, 187-195, doi: 10.1016/j.quaint.2014.06.064, 2014.**

530 Ma, L. J. and Qin, D. H.: Spatial-Temporal Characteristics of Observed Key Parameters for Snow
531 Cover in China during 1957-2009, *Journal of Glaciology and Geocryology*, 34, 1-11, 2012.

532 Michaelson, G. J., Ping, C., and Kimble, J.: Carbon storage and distribution in tundra soils of
533 Arctic Alaska, USA, *Arctic and Alpine Research*, 414-424, doi: 10.1023/A:1009731808445,

534 1996.

535 Morison, J., Aagaard, K., and Steele, M.: Recent environmental changes in the Arctic: a review,
536 Arctic, 359-371, 2000.

537 Mu, C., Zhang, T., Wu, Q., Cao, B., Zhang, X., Peng, X., Wan, X., Zheng, L., Wang, Q., and
538 Cheng, G.: Carbon and nitrogen properties of permafrost over the Eboling Mountain in the
539 upper reach of Heihe River basin, Northwestern China, Arctic, Antarctic, and Alpine Research,
540 47, 203-211, doi: 10.1657/AAAR00C-13-095, 2015.

541 Nelson, F. E.: (Un) frozen in time, Science, 299, 1673, 2003.

542 Nelson, F. E. and Outcalt, S. I.: A computational method for prediction and regionalization of
543 permafrost, Arctic and Alpine Research, 279-288, doi: 10.2307/1551363, 1987.

544 Osterkamp, T., Viereck, L., Shur, Y., Jorgenson, M., Racine, C., Doyle, A., and Boone, R.:
545 Observations of thermokarst and its impact on boreal forests in Alaska, USA, Arctic, Antarctic,
546 and Alpine Research, 303-315, doi: 10.2307/1552529, 2000.

547 Park, H., Fedorov, A. N., Zheleznyak, M. N., Konstantinov, P. Y., and Walsh, J. E.: Effect of snow
548 cover on pan-Arctic permafrost thermal regimes, Climate Dynamics, 44, 2873-2895, doi:
549 10.1007/s00382-014-2356-5, 2015.

550 Park, H., Kim, Y., and Kimball, J. S.: Widespread permafrost vulnerability and soil active layer
551 increases over the high northern latitudes inferred from satellite remote sensing and process
552 model assessments, Remote Sensing of Environment, 175:349-358, doi:
553 10.1016/j.rse.2015.12.046, 2016.

554 Park, H., Walsh, J., Fedorov, A., Sherstiukov, A., Iijima, Y., and Ohata, T.: The influence of
555 climate and hydrological variables on opposite anomaly in active-layer thickness between
556 Eurasian and North American watersheds, The Cryosphere, 7, 631-645, doi:
557 10.5194/tcd-6-2537-2012, 2013.

558 **Peng, S., Chen, A., Xu, L., Cao, C., Fang, J., Myneni, R. B., Pinzon, J. E., Tucker, C. J., and**
559 **Piao, S.: Recent change of vegetation growth trend in China, Environmental Research**
560 **Letters, 6, 044027, doi: 10.1088/1748-9326/6/4/044027, 2011.**

561 Peng, X., Zhang, T., Cao, B., Wang, Q., Wang, K., Shao, W., and Guo, H.: Changes in
562 freezing-thawing index and soil freeze depth over the Heihe River Basin, western China, Arctic,
563 Antarctic, and Alpine Research, 48, 161-176, doi: 10.1657/AAAR00C-13-127, 2016.

564 **Peng, X., Frauenfeld, O. W., Cao, B., Wang, K., Wang, H., Su, H., Huang, Z., Yue, D., and Zh**
565 **ang, T.: Response of changes in seasonal soil freeze/thaw state to climate change from 1950**
566 **to 2010 across china, Journal of Geophysical Research: Earth Surface, 121, 1984–2000,**
567 **doi: 10.1002/2016JF003876, 2016.**

568 Peng, X., Zhang, T., Zhong, X., Wang, Q., and Wang, K.: Spatial and temporal variations of NDVI
569 and its response to meteorological factors over Heihe River Basin of Qilian Mountains, Journal of
570 Lanzhou University (Natural Sciences), 49, 192-202, 2013.

571 Peterson, T. C., Vose, R., Schmoyer, R., and Razuvaev, V.: Global Historical Climatology Network
572 (GHCN) quality control of monthly temperature data, International Journal of Climatology, 18,
573 1169-1179, doi: 10.1002/(sici)1097-0088(199809)18:11<1169::aid-joc309>3.0.co;2-u, 1998.

574 Peterson, T. C. and Vose, R. S.: An overview of the Global Historical Climatology Network
575 temperature database, Bulletin of the American Meteorological Society, 78, 2837-2849, doi: An
576 overview of the Global Historical Climatology Network temperature database, 1997.

577 **Piao, S., Wang, X., Ciais, P., Zhu, B., Wang, T., and Liu, J.: Changes in satellite-derived**
578 **vegetation growth trend in temperate and boreal Eurasia from 1982 to 2006, Global**
579 **Change Biology, 17, 3228–3239, doi: 10.1111/j.1365-2486.2011.02419.x, 2011.**

580 Ravello, L., Allignol, F., Deline, P., Gruber, S., and Ravello, M.: Rock falls in the Mont Blanc
581 Massif in 2007 and 2008, Landslides, 7, 493-501, doi: 10.1007/s10346-010-0206-z, 2010.

582 Romanovsky, V. E., Smith, S. L., and Christiansen, H. H.: Permafrost thermal state in the polar
583 Northern Hemisphere during the international polar year 2007–2009: a synthesis, Permafrost
584 and Periglacial Processes, 21, 106-116, doi: 10.1002/ppp.689, 2010.

585 Sannel, A. and Kuhry, P.: Warming-induced destabilization of peat plateau/thermokarst lake
586 complexes, Journal of Geophysical Research: Biogeosciences, 116, doi:10.1029/2010JG001635,
587 2011.

588 Schuur, E. A., Bockheim, J., Canadell, J. G., Euskirchen, E., Field, C. B., Goryachkin, S. V.,
589 Hagemann, S., Kuhry, P., Lafleur, P. M., and Lee, H.: Vulnerability of permafrost carbon to
590 climate change: implications for the global carbon cycle, BioScience, 58, 701-714, doi:

591 10.1641/B580807, 2008.

592 Shiklomanov, N. and Nelson, F.: Active-layer mapping at regional scales: A 13-year spatial time
593 series for the Kuparuk region, north-central Alaska, Permafrost and Periglacial Processes, 13,
594 219-230, doi: 10.1002/ppp.425, 2002.

595 Shiklomanov, N. I.: Non-climatic factors and long-term, continental-scale changes in seasonally
596 frozen ground, Environmental Research Letters, 7, 011003, doi: 10.1088/1748-9326/7/1/011003,
597 2012.

598 Smith, S., Romanovsky, V., Lewkowicz, A., Burn, C., Allard, M., Clow, G., Yoshikawa, K., and
599 Throop, J.: Thermal state of permafrost in North America: a contribution to the international
600 polar year, Permafrost and Periglacial Processes, 21, 117-135, doi: 10.1002/ppp.690, 2010.

601 Smith, S. L. and Burgess, M. M.: Mapping the sensitivity of Canadian permafrost to climate
602 warming, IAHS PUBLICATION, 1999. 71-80, 1999.

603 Snyder, P., Delire, C., and Foley, J.: Evaluating the influence of different vegetation biomes on the
604 global climate, Climate Dynamics, 23, 279-302, doi: 10.1007/s00382-004-0430-0, 2004.

605 Stendel, M. and Christensen, J.: Impact of global warming on permafrost conditions in a coupled
606 GCM, Geophysical Research Letters, 29, doi: 10.1029/2001GL014345, 2002.

607 **Stocker, T. F., Qin, D., Plattner, G. K., Tignor, M. M. B., Allen, S. K., Boschung, J., Nauels, A.,**
608 **Xia, Y., Bex, V., and Midgley, P. M.: Climate Change 2013: The Physical Science Basis.**
609 **Contribution of Working Group I to the Fifth Assessment Report of IPCC the**
610 **Intergovernmental Panel on Climate Change, 2014.**

611 Streletskiy, D., Anisimov, O., Vasiliev, A., and Whiteman, C.: Permafrost degradation, Snow and
612 Ice-Related Hazards, Risks, and Disasters, 303, doi: 10.1016/B978-0-12-394849-6.00001-9,
613 2014.

614 Streletskiy, D. A., Sherstiukov, A. B., Frauenfeld, O. W., and Nelson, F. E.: Changes in the
615 1963–2013 shallow ground thermal regime in Russian permafrost regions, Environmental
616 Research Letters, 10, 125005, doi: 10.1088/1748-9326/10/12/125005, 2015a.

617 Streletskiy, D. A., Tananaev, N. I., Opel, T., Shiklomanov, N. I., Nyland, K. E., Streletskaya, I. D.,
618 and Shiklomanov, A. I.: Permafrost hydrology in changing climatic conditions: seasonal
619 variability of stable isotope composition in rivers in discontinuous permafrost, Environmental
620 Research Letters, 10, 095003, doi: 10.1088/1748-9326/10/9/095003, 2015b.

621 Swann, A. L., Fung, I. Y., Levis, S., Bonan, G. B., and Doney, S. C.: Changes in Arctic vegetation
622 amplify high-latitude warming through the greenhouse effect, Proceedings of the National
623 Academy of Sciences, 107, 1295-1300, doi: 10.1073/pnas.0913846107, 2010.

624 Tourre, Y., Jarlan, L., Lacaux, J., Rotela, C., and Lafaye, M.: Spatio-temporal variability of
625 NDVI–precipitation over southernmost South America: possible linkages between climate
626 signals and epidemics, Environmental Research Letters, 3, 044008, doi:
627 10.1088/1748-9326/3/4/044008, 2008.

628 Wang, G., Hu, H., and Li, T.: The influence of freeze–thaw cycles of active soil layer on surface
629 runoff in a permafrost watershed, Journal of Hydrology, 375, 438-449, doi:
630 10.1016/j.jhydrol.2009.06.046, 2009.

631 Wang, K., Zhang, T., and Zhong, X.: Changes in the timing and duration of the near-surface soil
632 freeze/thaw status from 1956 to 2006 across China, The Cryosphere, 9, 1321-1331, doi:
633 10.5194/tc-9-1321-2015, 2015.

634 Willmott, C. J. and Matsuura, K.: Smart interpolation of annually averaged air temperature in the
635 United States, Journal of Applied Meteorology, 34, 2577-2586, doi:
636 10.1175/1520-0450(1995)034<2577:sioaaa>2.0.co;2, 1995.

637 Willmott, C. J. and Robeson, S. M.: Climatologically aided interpolation (CAI) of terrestrial air
638 temperature, International Journal of Climatology, 15, 221-229, doi: 10.1002/joc.3370150207,
639 1995.

640 Wu, Q., Hou, Y., Yun, H., and Liu, Y.: Changes in active-layer thickness and near-surface
641 permafrost between 2002 and 2012 in alpine ecosystems, Qinghai–Xizang (Tibet) Plateau,
642 China, Global and Planetary Change, 124, 149-155, doi: 10.1002/joc.3370150207, 2015.

643 Wu, Q. and Zhang, T.: Recent permafrost warming on the Qinghai-Tibetan Plateau, Journal of
644 Geophysical Research: Atmospheres, 113, doi:10.1029/2007JD009539, 2008.

645 Wu, Q., Zhang, T., and Liu, Y.: Permafrost temperatures and thickness on the Qinghai-Tibet
646 Plateau, Global and Planetary Change, 72, 32-38, doi: 10.1016/j.gloplacha.2010.03.001, 2010.

647 Wu, T., Wang, Q., Zhao, L., Batkhisig, O., and Watanabe, M.: Observed trends in surface

648 freezing/thawing index over the period 1987–2005 in Mongolia, *Cold Regions Science and*
649 *Technology*, 69, 105-111, doi: 10.1016/j.coldregions.2011.07.003, 2011.

650 **Zhang, G., Zhang, Y., Dong, J., and Xiao, X.: Green-up dates in the Tibetan Plateau have**
651 **continuously advanced from 1982 to 2011, *Proceedings of the National Academy of***
652 ***Sciences*, 110, 4309-4314, doi: 10.1073/pnas.1210423110, 2013.**

653 Zhang, T.: Influence of the seasonal snow cover on the ground thermal regime: An overview,
654 *Reviews of Geophysics*, 43, doi: 10.1029/2004RG000157, 2005.

655 Zhang, T., Armstrong, R., and Smith, J.: Investigation of the near-surface soil freeze-thaw cycle in
656 the contiguous United States: Algorithm development and validation, *Journal of Geophysical*
657 *Research: Atmospheres*, 108, doi: 10.1029/2003JD003530, 2003.

658 Zhang, T., Barry, R. G., and Armstrong, R. L.: Application of satellite remote sensing techniques
659 to frozen ground studies, *Polar Geography*, 28, 163-196, doi: 10.1080/789610186, 2004.

660 Zhang, T., Barry, R. G., Knowles, K., Heginbottom, J., and Brown, J.: Statistics and characteristics
661 of permafrost and ground-ice distribution in the Northern Hemisphere, *Polar Geography*, 23,
662 132-154, doi: 10.1080/10889379909377670, 1999.

663 Zhang, T., Frauenfeld, O. W., Serreze, M. C., Etringer, A., Oelke, C., McCreight, J., Barry, R. G.,
664 Gilichinsky, D., Yang, D., and Ye, H.: Spatial and temporal variability in active layer thickness
665 over the Russian Arctic drainage basin, *Journal of Geophysical Research: Atmospheres*, 110,
666 doi: 10.1029/2004JD005642, 2005.

667 Zhang, T., Osterkamp, T., and Stamnes, K.: Effects of climate on the active layer and permafrost
668 on the North Slope of Alaska, USA, *Permafrost and Periglacial Processes*, 8, 45-67, doi:
669 10.1002/(SICI)1099-1530(199701)8:1<45::AID-PPP240>3.0.CO;2-K, 1997.

670 Zhang, T. and Stamnes, K.: Impact of climatic factors on the active layer and permafrost at Barrow,
671 Alaska, *Permafrost and Periglacial Processes*, 9, 229-246, doi:
672 10.1002/(SICI)1099-1530(199807/09)9:3<229::AID-PPP286>3.0.CO;2-T, 1998.

673 Zhang, T., Stamnes, K., and Bowling, S.: Impact of the atmospheric thickness on the atmospheric
674 downwelling longwave radiation and snowmelt under clear-sky conditions in the Arctic and
675 Subarctic, *Journal of Climate*, 14, 920-939, doi:
676 10.1175/1520-0442(2001)014<0920:IOTATO>2.0.CO;2, 2001.

677 Zhang, X. M., Sheng, Y., Wu, J. C., Chen, J., Li, J., Cao, Y. B., and Li, K.: Changes of species
678 diversity indices along the ground temperature of permafrost in the source region of Datong
679 River in the Qilian Mountains, northwestern China, *Journal of Beijing Forestry University*, 34,
680 86-93, 2012.

681 Zhao, L., Ping, C. L., Yang, D., Cheng, G., Ding, Y., and Liu, S.: Changes of climate and
682 seasonally frozen ground over the past 30 years in Qinghai–Xizang (Tibetan) Plateau, China,
683 *Global and Planetary Change*, 43, 19-31, doi: 10.1016/j.gloplacha.2004.02.003, 2004.

684 Zhao, L., Wu, Q., Marchenko, S., and Sharkhuu, N.: Thermal state of permafrost and active layer
685 in Central Asia during the International Polar Year, *Permafrost and Periglacial Processes*, 21,
686 198-207, doi: 10.1002/ppp.688, 2010.

687 Zhong, X., Zhang, T., and Wang, K.: Snow density climatology across the former USSR, *The*
688 *Cryosphere*, 8, 785-799, doi: 10.5194/tc-8-785-2014, 2014.

689 Zhou, Y., Guo, D., Qiu, G., and Cheng, G.: *Frozen Ground in China*, Science Press, Beijing, 450pp,
690 2000.

691 **Zhu, Z., Piao, S., Myneni, R. B., Huang, M., Zeng, Z., Canadell, J. G., Ciais, P., Sitch, S.,**
692 **Friedlingstein, P., and Arneth, A.: Greening of the Earth and its drivers, *Nature Climate***
693 ***Change*, 6, doi:10.1038/nclimate3004, 2016.**

694

695

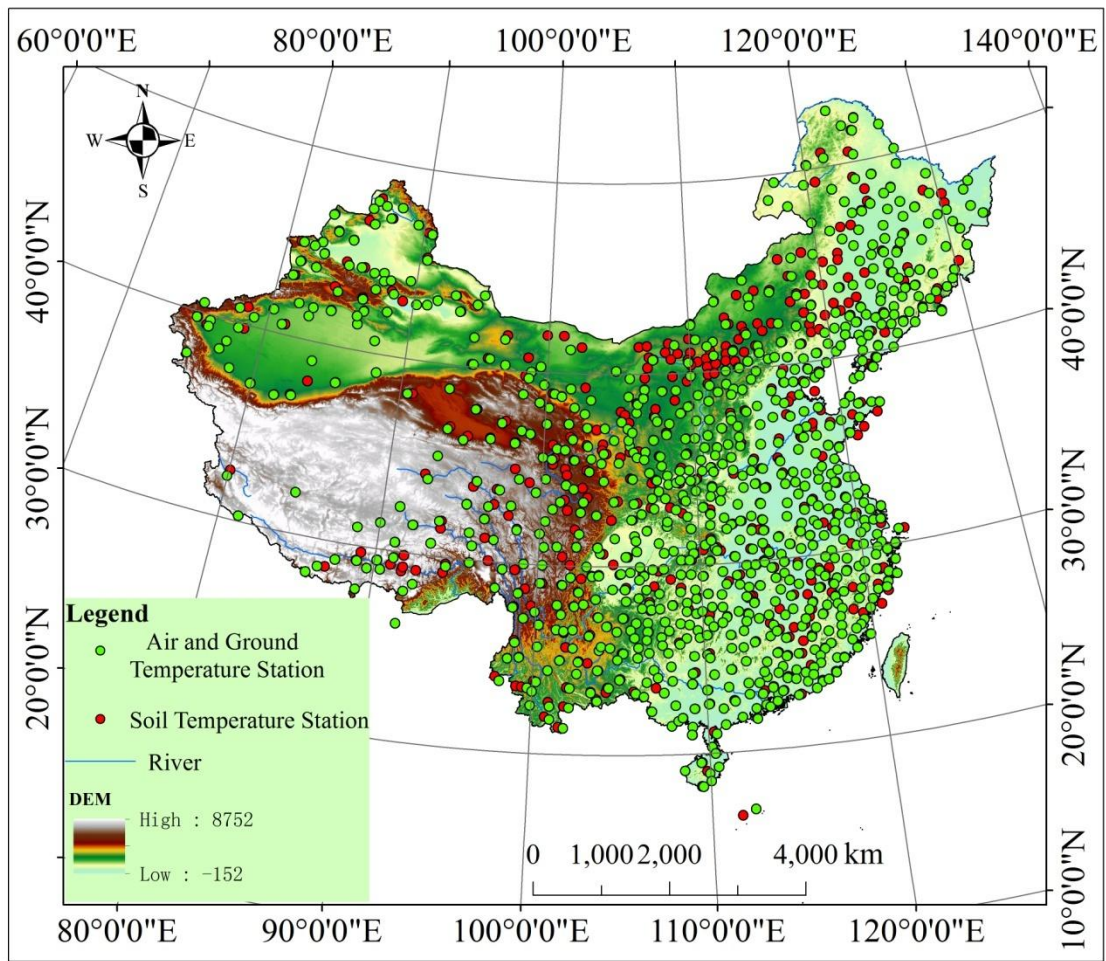
696

697

698

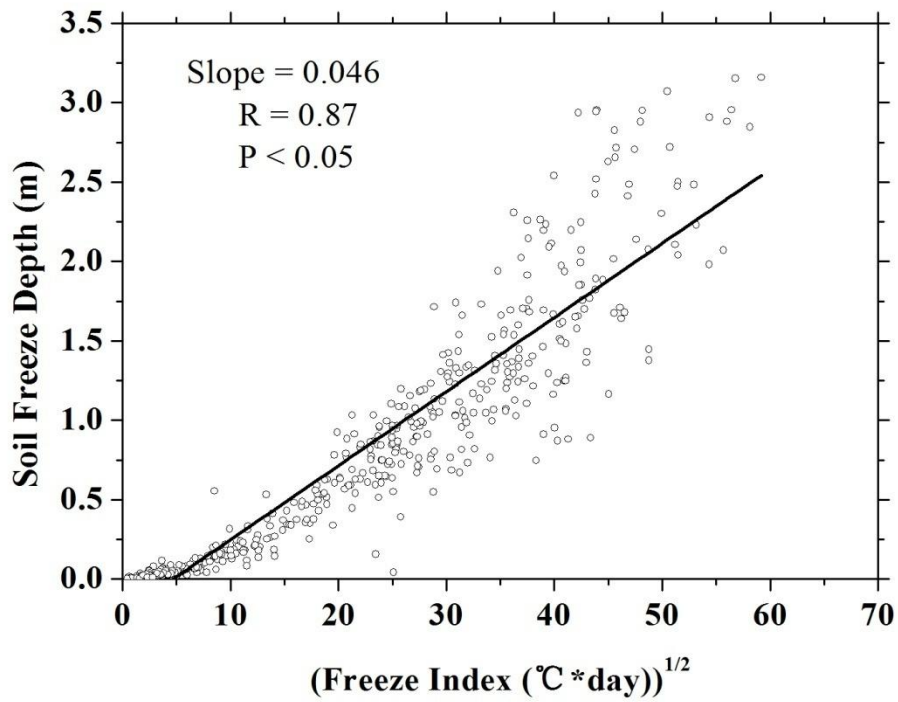
699

700 **Figure captions:**
701 **Figure 1.** The observational station distribution across China, including the 839 stations with air
702 and ground surface temperatures (green symbols), 845 soil temperature stations (red symbols), and
703 elevation. The blue solid lines represent the main rivers.
704 **Figure 2.** Linear least squares regression between soil freeze depth and annual freezing index
705 based on observational sites. The black solid line represents the linear regression.
706 **Figure 3.** Comparison of the simulated and observed SFD for all stations. The black solid line is
707 the 1:1 line, while the gray dashed line is regression fit between the simulated and observed
708 values.
709 **Figure 4.** Spatial distribution and variability of SFD at the observing stations. (a) Multi-year mean
710 SFD at each site; (b) the number of sites contributing to the SFD mean; (c) the magnitude of SFD
711 change at each site; (d) the number of sites with SFD change observations.
712 **Figure 5.** The standard deviation of SFD at each site across China.
713 **Figure 6.** 1951–2012 SFD anomalies with respect to the 1971–2000 mean (red solid line) based
714 on up to 839 stations across China as depicted in figure 1. Included also is the 1 standard deviation
715 range (gray shading), the linear trend from 1967 to 2012 (blue dashed line), and the 7-year
716 smoothing (green line). The inset shows the number of stations contributing to the time series.
717 **Figure 7.** Spatial variability of SFD in the decades of the 1950s, 1960s, 1970s, 1980s, 1990s, and
718 2000s across China.
719 **Figure 8.** SFD trends across China from 1950 to 2009. The grey regions indicate non-significant
720 SFD changes, while trends in all other regions are statistically significant.
721 **Figure 9.** SFD time series and trend (black) and the potential forcing variables: (a) mean annual
722 ground surface temperature (red), (b) mean annual air temperature (green), (c) surface freeze
723 index (cyan), (d) air freezing index (magenta), (e) surface thawing index (yellow), (f) air thawing
724 index (orange). All variables are standardized to range from 0–1. R is the correlation coefficient,
725 and all are statistically significant.
726 **Figure 10.** Correlation between SFD and SND. The variables are standardized to range from 0–1.
727 **Figure 11.** Correlation between SFD and mean annual NDVI.
728 **Figure 12.** Time-series of SFD changes in different climate zones: (a) subtropical monsoon, (b)
729 temperate monsoon, (c) temperate continent, (d) Qinghai-Tibetan Plateau Alpine, and (e) tropical.
730 The insets are the SFD changes in the four climate zones; the bold black line is SFD, and bold red
731 line is the trend.
732
733
734



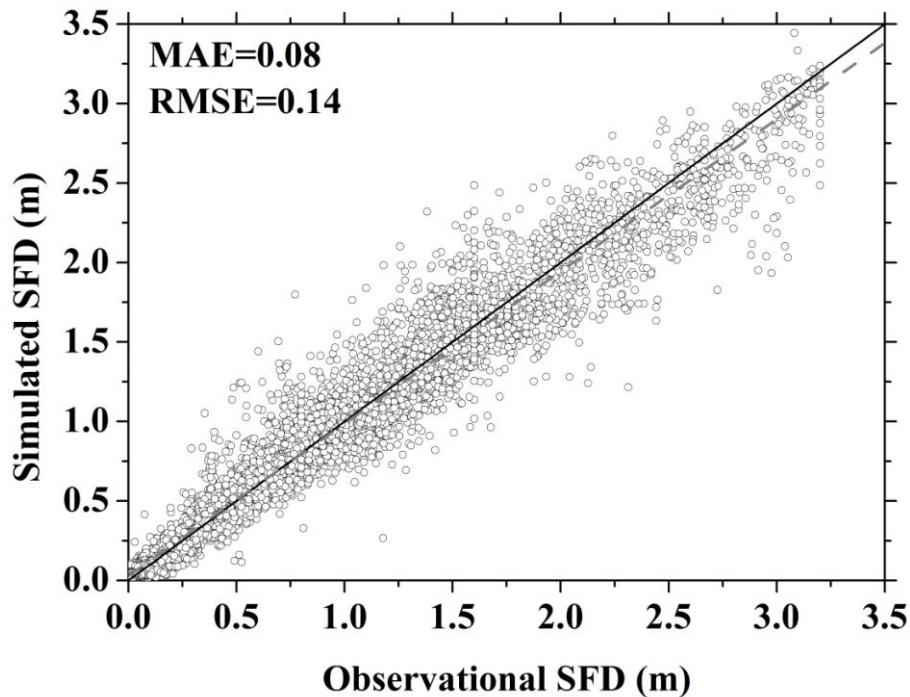
735
736
737
738
739

Figure 1. The observational station distribution across China, including the 839 stations with air and ground surface temperatures (green symbols), 845 soil temperature stations (red symbols), and elevation. The blue solid lines represent the main rivers.



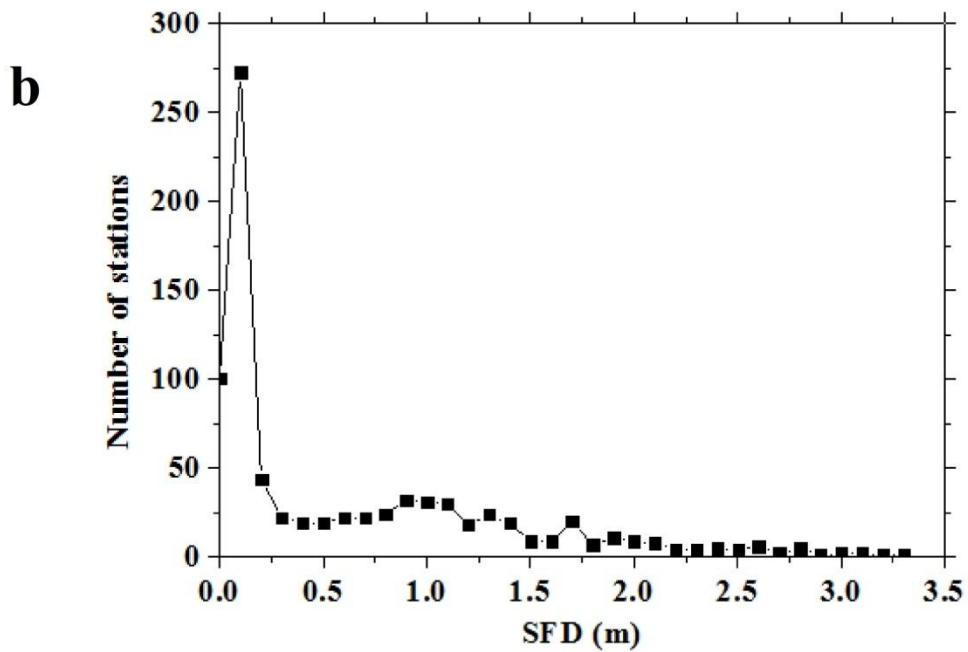
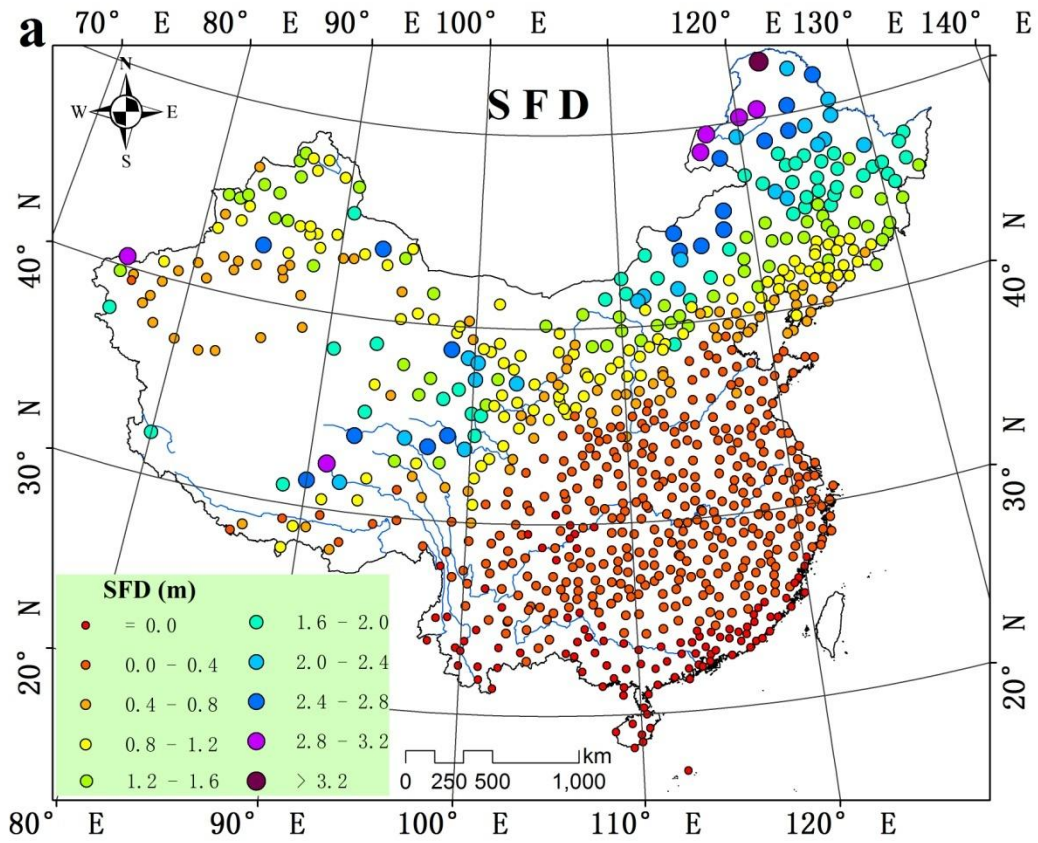
740
741
742

Figure 2. Linear least squares regression between soil freeze depth and annual freezing index based on observational sites. The black solid line represents the linear regression.

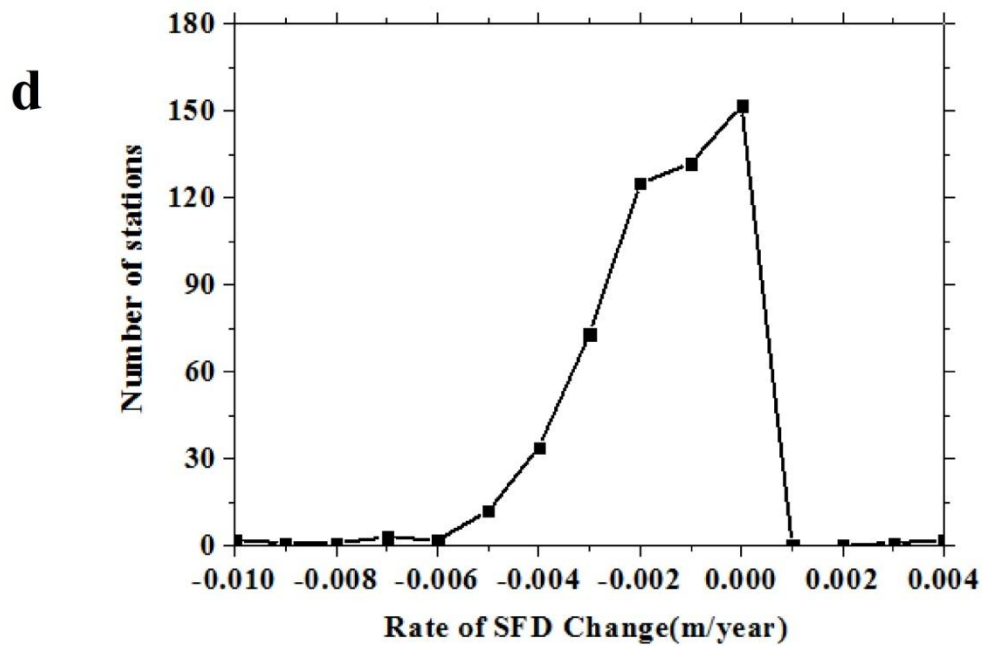
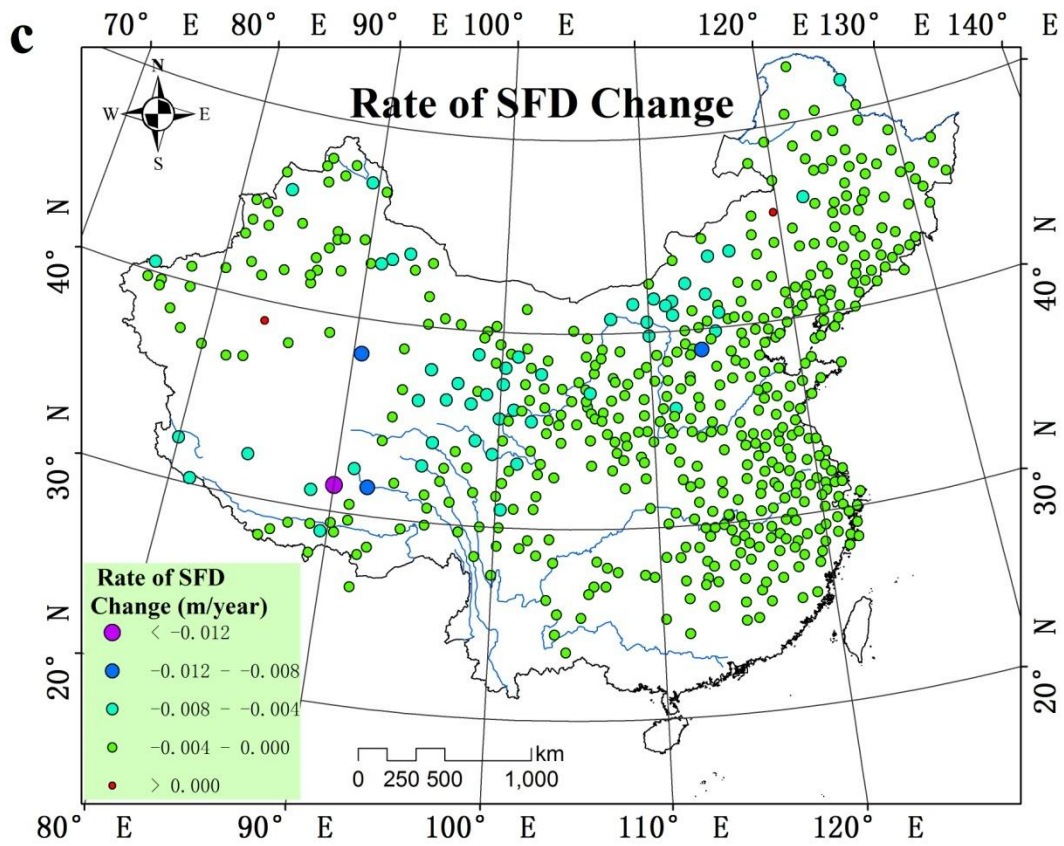


743
744
745
746
747
748
749

Figure 3. Comparison of the simulated and observed SFD for all stations. The black solid line is the 1:1 line, while the gray dashed line is regression fit between the simulated and observed values.



750



751
 752 **Figure 4.** Spatial distribution and variability of SFD at the observing stations. (a) Multi-year mean
 753 SFD at each site; (b) the number of sites contributing to the SFD mean; (c) the magnitude of SFD
 754 change at each site; (d) the number of sites with SFD change observations.
 755

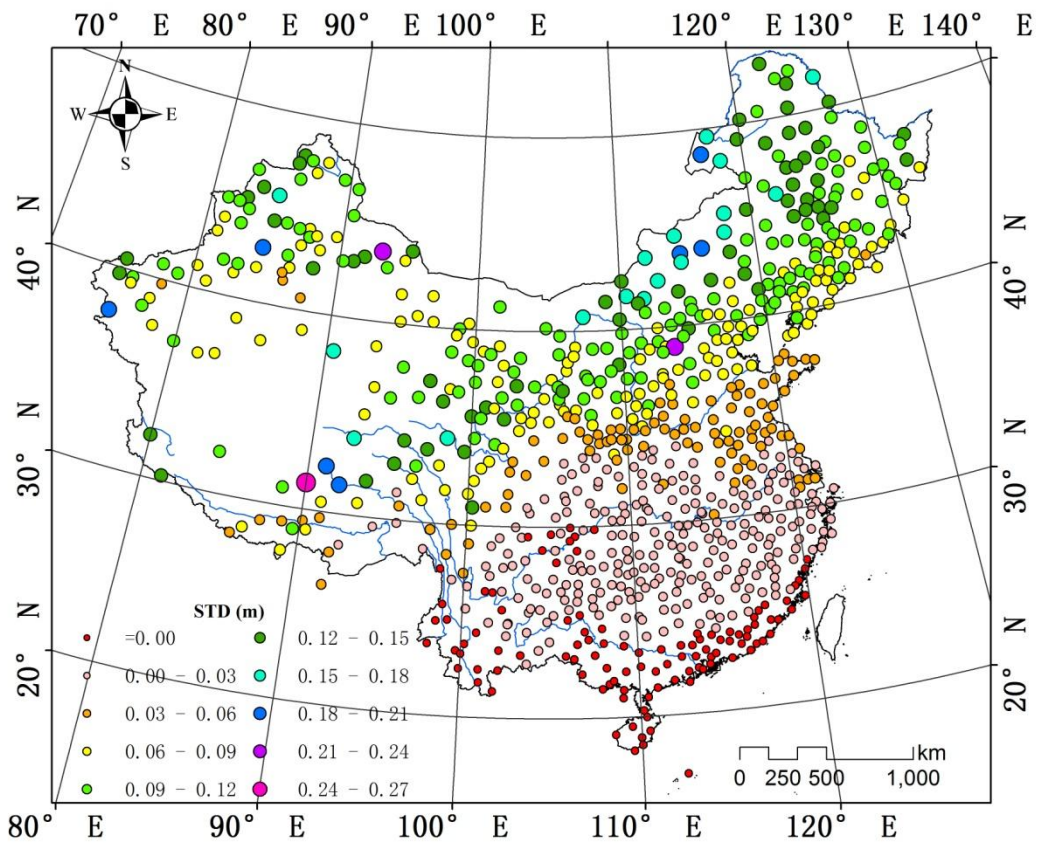
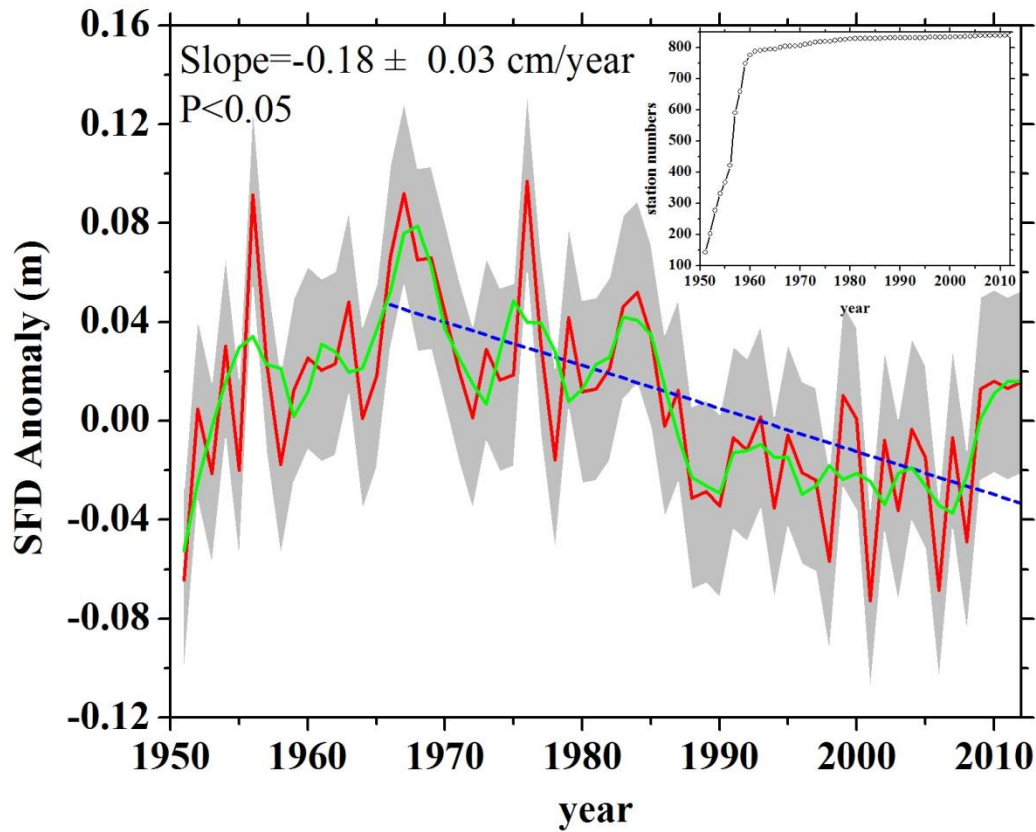


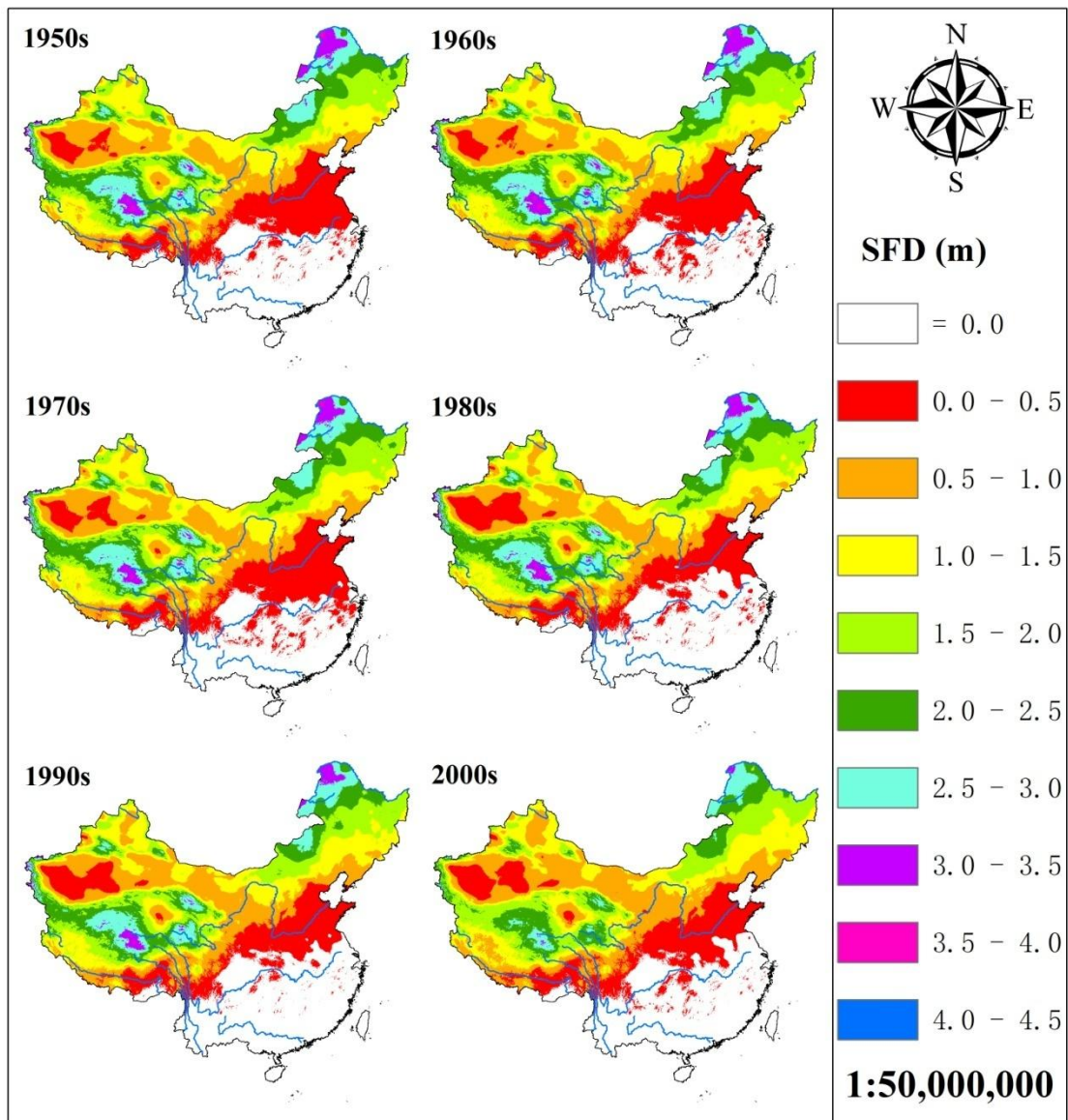
Figure 5. The standard deviation of SFD at each site across China.

757
758
759
760
761



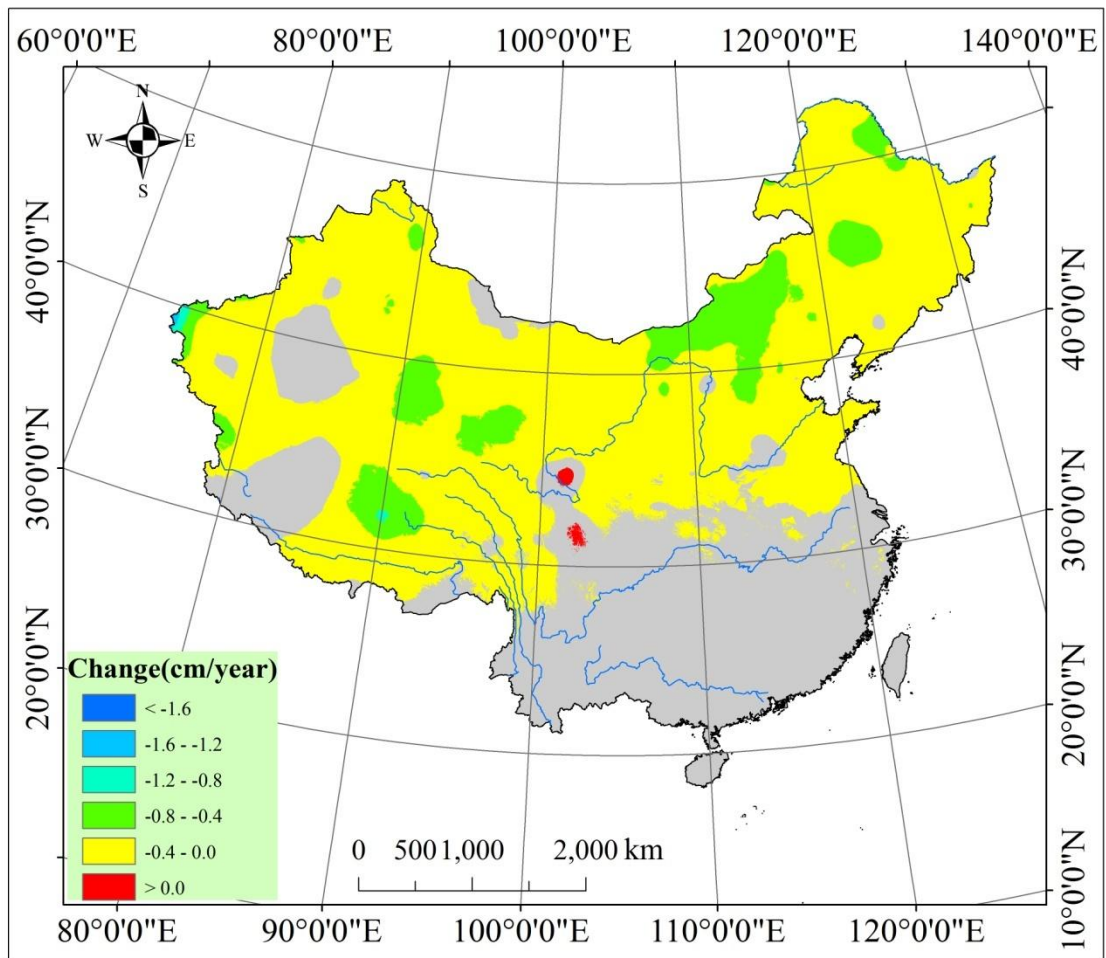
762
 763
 764
 765
 766
 767

Figure 6. 1951–2012 SFD anomalies with respect to the 1971–2000 mean (red solid line) based on up to 839 stations across China as depicted in figure 1. Included also is the 1 standard deviation range (gray shading), the linear trend from 1967 to 2012 (blue dashed line), and the 7-year smoothing (green line). The inset shows the number of stations contributing to the time series.



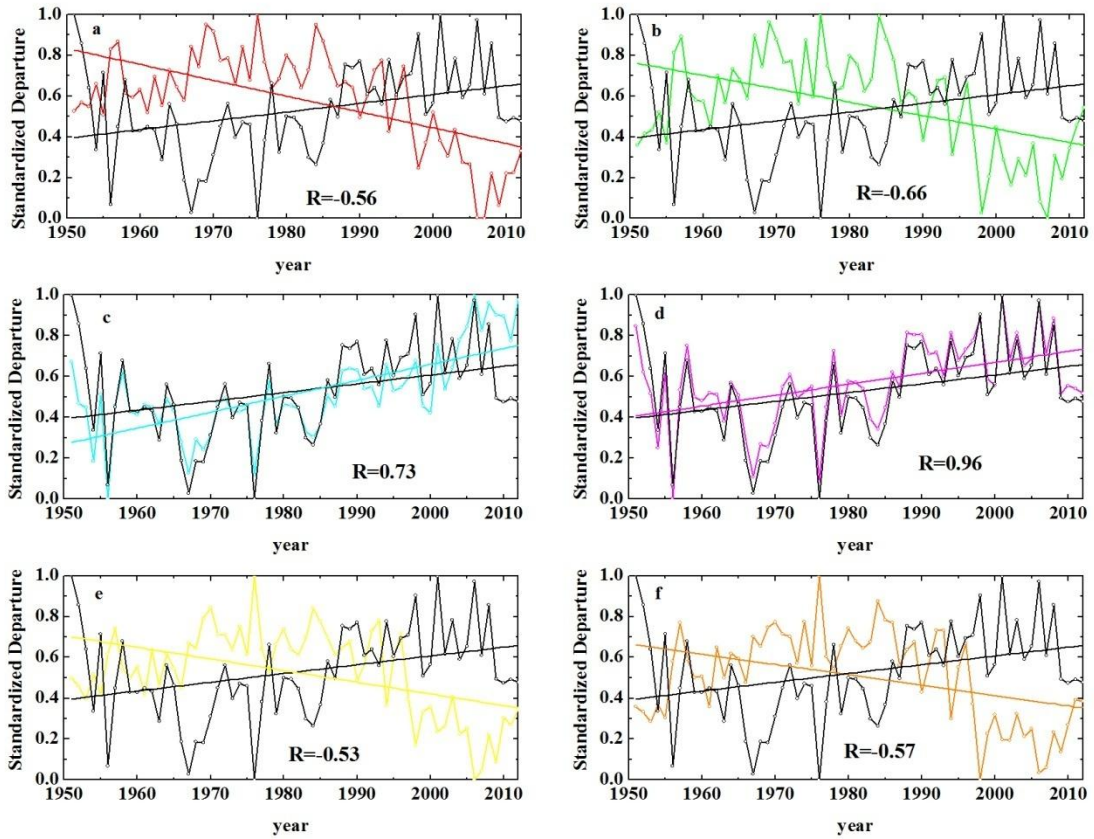
768
769
770

Figure 7. Spatial variability of SFD in the decades of the 1950s, 1960s, 1970s, 1980s, 1990s, and 2000s across China.



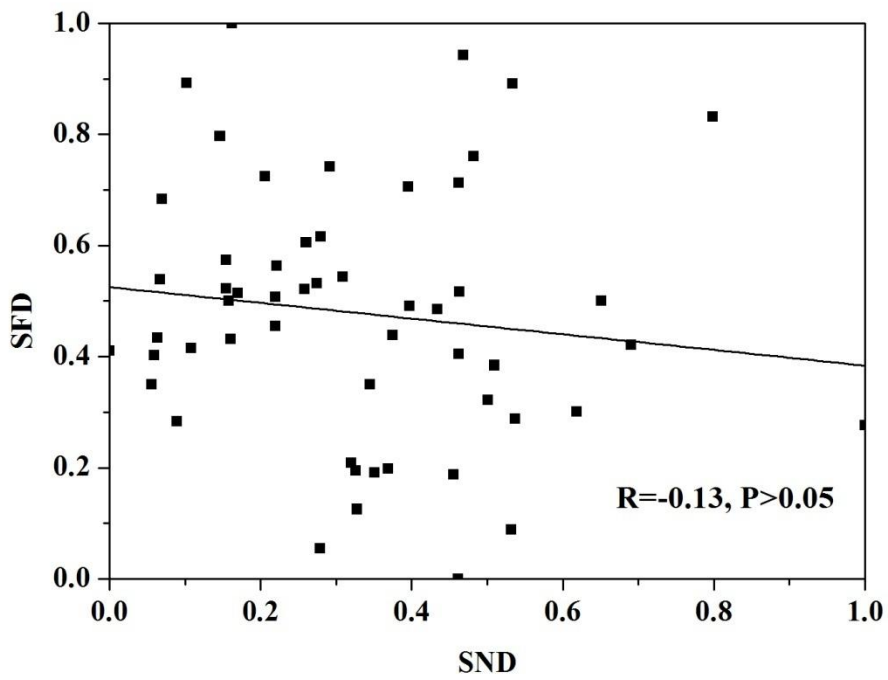
771
772
773
774

Figure 8. SFD trends across China from 1950 to 2009. The grey regions indicate non-significant SFD changes, while trends in all other regions are statistically significant.



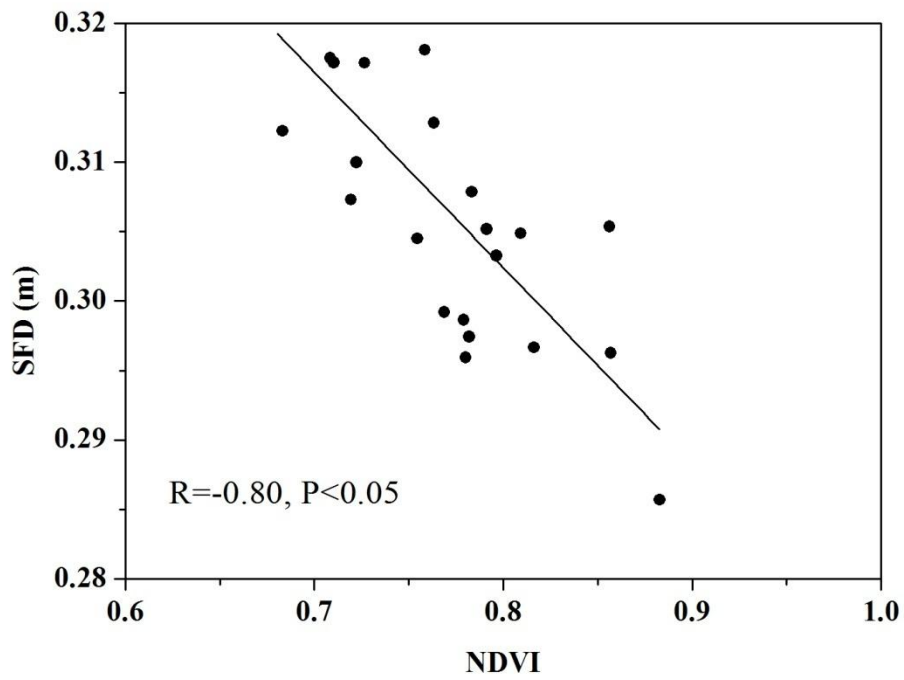
775
 776
 777
 778
 779
 780
 781
 782
 783

Figure 9. SFD time series and trend (black) and the potential forcing variables: (a) mean annual ground surface temperature (red), (b) mean annual air temperature (green), (c) surface freeze index (cyan), (d) air freezing index (magenta), (e) surface thawing index (yellow), (f) air thawing index (orange). All variables are standardized to range from 0–1. R is the correlation coefficient, and all are statistically significant.



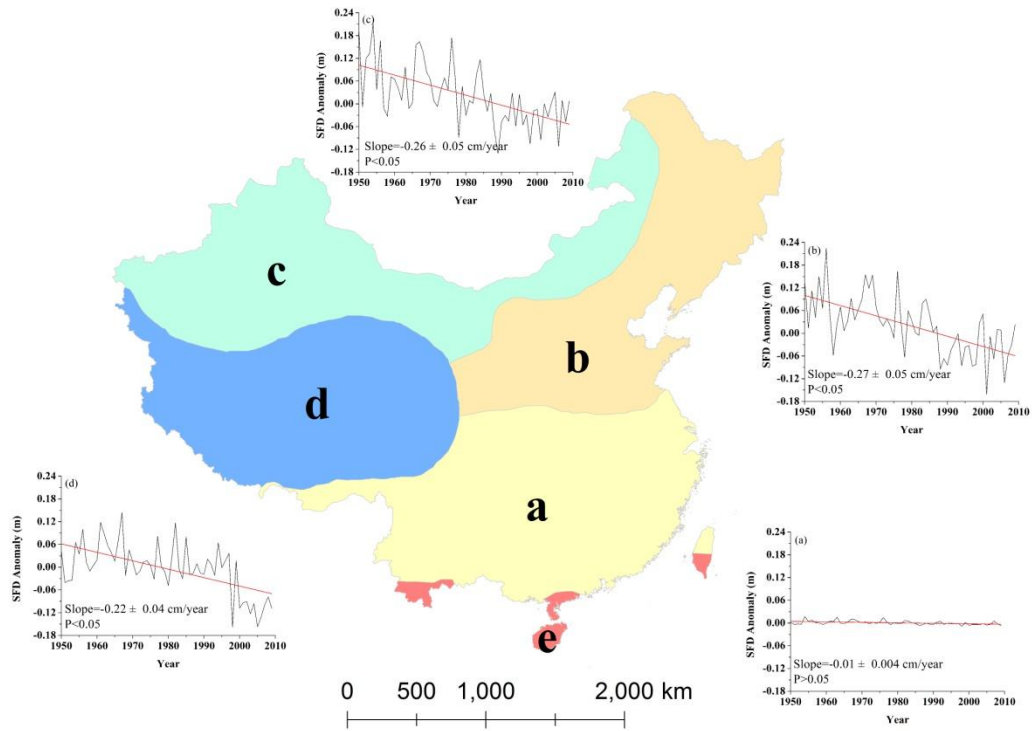
784
785
786
787
788
789
790
791
792
793
794

Figure 10. Correlation between SFD and SND. The variables are standardized to range from 0–1.



795
 796
 797
 798
 799
 800
 801
 802
 803
 804
 805

Figure 11. Correlation between SFD and mean annual NDVI.



806
807
808
809
810

Figure 12. Time-series of SFD changes in different climate zones: (a) subtropical monsoon, (b) temperate monsoon, (c) temperate continent, (d) Qinghai-Tibetan Plateau Alpine, and (e) tropical. The insets are the SFD changes in the four climate zones; the bold black line is SFD, and bold red line is the trend.